



1 **Vegetation and geochemical responses to Holocene rapid**
2 **climate change in Sierra Nevada (SE Iberia): The Laguna**
3 **Hondera record**

4 Jose Manuel Mesa-Fernández^{1, 2}, Gonzalo Jiménez-Moreno¹, Marta Rodrigo-Gámiz²,
5 Antonio García-Alix^{1,2}, Francisco J. Jiménez-Espejo³, Francisca Martínez-Ruiz², R.
6 Scott Anderson⁴, Jon Camuera¹ and María J. Ramos-Román¹

7 ¹ Departamento de Estratigrafía y Paleontología, Universidad de Granada (UGR), Avda. Fuente Nueva
8 s/n, 18002, Granada, Spain

9 ² Instituto Andaluz de Ciencias de la Tierra (IACT), CSIC-UGR, Avenida de las Palmeras 4, 18100,
10 Armilla, Granada, Spain

11 ³ Department of Biogeochemistry (JAMSTEC), Yokosuka, Japan.

12 ⁴ School of Earth Sciences and Environmental Sustainability, Northern Arizona University, Flagstaff,
13 AZ, USA.

14 *Correspondance to:* Jose Manuel Mesa-Fernández (jimesa@iact.ugr-csic.com)

15 **Abstract.**

16 High-altitude peat bogs and lacustrine records are very sensitive to climate changes and atmospheric
17 pollution. Recent studies show a close relationship between regional climate aridity and enhanced eolian
18 input to lake sediments. However, changes in regional-scale dust fluxes due to climate variability at short-
19 scales and how alpine environments were impacted by climatic- and human-induced environmental
20 changes are not completely understood.

21 Here we present a multi-proxy lake sediment record of climate variability in the Sierra Nevada (SE
22 Iberian Peninsula) over the Holocene. Palynological, geochemical and magnetic susceptibility (MS)
23 proxies obtained from the high mountain lake record of Laguna Hondera (LH) evidence humid conditions
24 during the Early Holocene, while a trend towards more arid conditions is recognized since ~7000 cal yr
25 BP, with enhanced Saharan eolian dust deposition until Present. This trend towards enhanced arid
26 conditions was modulated by millennial-scale climate variability. Relative humid conditions occurred
27 during the Iberian Roman Humid Period (2600-1450 cal yr BP) and predominantly arid conditions
28 occurred during the Dark Ages and the Medieval Climate Anomaly (1450-650 cal yr BP). The Little Ice
29 Age (650-150 cal yr BP) is characterized in the LH record by an increase in runoff and a minimum in
30 eolian input. In addition, human impact in the area is noticed through the record of *Olea* cultivation,
31 *Pinus* reforestation and Pb pollution during the Industrial Period (150 cal yr BP-present). Furthermore, a
32 unique feature preserved at LH is the correlation between Zr and Ca, two important elements of Saharan
33 dust source in Sierra Nevada lake records. This supports that present day biochemical observations,
34 pointing to eolian input as main inorganic nutrient source for oligotrophic mountain lakes, are comparable
35 to the past record of eolian supply to these high-altitude lakes.

36 **1. Introduction**

37 Southern Spain has been the location for a number of recent studies detailing past vegetation and former
38 climate of the region (Carrión et al., 2001, 2003, 2007, 2010; Carrión, 2002; Combourieu Nebout et al.,
39 2009; Jiménez-Espejo et al., 2008; Martín-Puertas et al., 2008, 2010; Fletcher et al., 2010; Nieto-Moreno



40 et al., 2011, 2015; Rodrigo-Gámiz et al., 2011; Moreno et al., 2012 Jiménez-Moreno et al., 2015). These
41 studies have documented that the western Mediterranean area has been very sensitive to short-term
42 climatic fluctuations throughout the Holocene (e.g., Fletcher and Sánchez-Goñi, 2008; Combourieu
43 Nebout et al., 2009; Fletcher et al., 2010; Jiménez-Moreno et al., 2013). However, a subset of recent
44 studies have attempted to determine how Mediterranean alpine environments have been affected by
45 Holocene climate change through the study of sedimentary records from high elevation wetlands in the
46 Sierra Nevada (Anderson et al., 2011; García-Alix et al., 2012, 2013; Jiménez-Moreno and Anderson,
47 2012; Jiménez-Moreno et al., 2013; Jiménez-Espejo et al., 2014; Ramos-Román et al., 2016; García-Alix
48 et al., 2017). These alpine lake and bog records show minimal anthropic influence because they are
49 usually elevational higher than major regional Late Holocene human landscape modification. This allows
50 for a potentially clearer climatic signal to be determined from these sites. However, even though human
51 impact is less important at high-elevations, the impacts of human activities has been reconstructed from
52 these Late Holocene sedimentary records (Anderson et al., 2011; García-Alix et al., 2012, 2013; 2017).
53 Recent studies have highlighted the role of atmospheric mineral dust deposition in marine (Pulido-Villena
54 et al., 2008a) and terrestrial (Morales-Baquero et al., 1999; Ballantyne et al., 2011) ecosystem fertilization
55 through major micronutrients supply. Similar results have been described in the Sierra Nevada alpine
56 lakes, where Saharan dust is especially important in conditioning plankton communities from oligotrophic
57 lakes (Morales-Baquero et al., 2006a, 2006b; Mladenov et al., 2008; Pulido-Villena et al., 2008b; Reche
58 et al., 2009). Although this eolian signal has been occasionally recorded in the sedimentary sequences
59 from the Sierra Nevada lakes (Jimenez-Espejo et al., 2014; García-Alix et al., 2017), the record of
60 inorganic nutrients in Saharan dust input in past lake geochemistry has remained elusive. This study
61 investigates a multiproxy sediment core record from Laguna Hondera (LH), located in the Sierra Nevada
62 range with three main goals: (1) identifying and characterizing climatic variability during the Holocene,
63 focusing on vegetation changes, eolian input and runoff sediments variations; (2) understanding the
64 Saharan dust influence in past lake sedimentation and geochemistry, and (3) investigating the
65 anthropogenic impact in the area.

66 2. Study Area

67 Sierra Nevada is the highest mountain ranges in the southern Iberian Peninsula. Bedrock of the high
68 elevations of the Sierra Nevada is mostly composed of metamorphic rocks, principally mica schists
69 (Castillo Martín, 2009). During the late Pleistocene, the Sierra Nevada was one of the southernmost
70 mountains to support alpine glaciers and its last advance was recorded during the Little Ice Age (LIA;
71 Palma et al., 2017; Oliva et al., 2018). Subsequently to the melting of ice at the end of the Last Glacial
72 Maximum, wetlands and small lakes formed in the glacial cirque basins, which occur between 2451-3227
73 masl (Schulte, 2002; Castillo Martín, 2009; Palma et al., 2017). Several alpine wetland and lakes have
74 been studied in this area during the last few years as shown in Figure 1.

75 2.1. Regional Climate and Vegetation

76 Mediterranean climate characterises southern Iberia, with a marked seasonal variation between warm and
77 dry summers and cool and humid winters (e.g. Lionello et al., 2006). Overprinting this general climate is



78 the influence of the North Atlantic Oscillation (NAO) (Trigo et al., 2004; Trouet et al., 2009). Southern
79 Iberia is also characterized by strong altitudinal contrasts, which in turn controls the precipitation
80 patterns, with mean annual values ranging from <400mm yr⁻¹ to >1400 mm yr⁻¹ in the southeast desert
81 lowlands and the southwest highland, respectively (Jiménez-Moreno et al., 2013 and references therein),
82 demonstrating the complexity of climate regime in this area.

83 As with most mountainous regions, species and species groupings in the Sierra Nevada are distributed
84 with respect to elevation, depending on the temperature and rainfall gradients (e.g., El Aallali et al., 1998;
85 Valle, 2003). Above 2800 m the crioromediterranean flora occurs as tundra-like open grassland. The
86 oromediterranean belt (1900 -2800 m), mostly includes dwarf *Juniperus* (juniper), xerophytic shrublands
87 and pasturelands and *Pinus sylvestris* and *P. nigra*. The supramediterranean belt (~1400 - 1900 m) is
88 characterized by mixed deciduous and evergreen forest species (i.e., evergreen and deciduous *Quercus*,
89 with *Pinus spp.* and others). Mesomediterranean vegetation (600 – 1400 m), includes sclerophyllous
90 shrublands and evergreen *Quercus* woodlands. The natural vegetation has been strongly altered by human
91 activities and cultivation in the last centuries, increasing significantly the abundance of *Olea* (olive), due
92 to cultivation at lower altitudes (Anderson et al., 2011, and references therein), and *Pinus* due to
93 reforestation primarily at higher elevations (Valbuena-Carabaña, 2010).

94 2.2. Laguna Hondera

95 Laguna Hondera (hereafter LH; 2899 masl; 37°02.88'N, 3°17.66'W, Fig. 1) is a small and shallow lake
96 located at the lowest elevation of a set of lakes locally named Cañada de Siete Lagunas, a glacial valley
97 between two of the highest peaks of the mountain range in the Iberian Peninsula: Alcazaba (3366m) and
98 Mulhacén (3479m). LH has a large catchment area (154.6 ha) compared with previously studied Sierra
99 Nevada wetlands (Laguna de Río Seco, LdRS, 9.9 ha; Borreguil de la Caldera, BdlC, 62 ha; Morales-
100 Baquero et al., 1999; Ramos-Román et al., 2016). The lake was reduced to a little pond in the deepest
101 area of the basin when cored in September 2012, with a maximum depth of only a few centimetres.

102 LH presently occurs in the crioromediterranean vegetation belt (2800 m) (El Aallali et al., 1998; Valle et
103 al., 2003). The bedrock in the LH basin consists in Paleozoic and Precambrian mica schist with disthene
104 and staurolite of the lower part of the Caldera Formation (Díaz de Federico et al., 1980).

105 3. Methods

106 3.1. Core sampling, lithology and chronology

107 Six sediment cores were recovered from LH with a Livingstone piston corer in September 2012. LH 12-
108 03 (83cm) was selected for a multiproxy study because it was the longest core. Cores were wrapped with
109 tin foil and plastic film and transported to Universidad de Granada, where they were stored at 4°C.

110 Core LH 12-03 was split longitudinally and the sediment features described. The magnetic susceptibility
111 was measured every 0.5 cm with a Bartington MS2E meter in SI units (x 10⁻⁴) along the entire LH 12-03
112 core (Fig. 2). The sediment cores were subsampled every 1 cm for different analyses, i.e., one portion for
113 pollen and another for geochemical analysis.



114 The age model was built using seven AMS radiocarbon dates from vegetal remains (Table 1; Fig. 2) by
115 means of Clam software (Blaauw, 2010; version 2.2), which used the IntCal13 curve for radiocarbon age
116 calibration (Reimer et al., 2013). The smooth spline approach was chosen (Fig. 2). The sediment
117 accumulation rate (SAR) was calculated with the average rate from the Clam smooth spline output (Fig.
118 2).

119 3.2. Pollen

120 Pollen analysis was performed on 1 cm³ of sample collected at regular 1cm interval throughout the first
121 62 cm of the core. Older sediments (from 62 to 82 cm depth) were barren in pollen, and only one interval
122 at 73 cm could be studied (Fig. 2). Pollen extraction included HCl and HF treatment, sieving, and the
123 addition of Lycopodium spores for calculation of pollen concentration (modified from Faegri and Iversen,
124 1989). Sieving was done using a 10- μ m nylon sieve. The resulting pollen residue was suspended in
125 glycerine and mounted on microscope slides. Slides were analysed at 400x magnification counting a
126 minimum of 300 pollen grains, not including the local aquatic species Cyperaceae, Ranunculaceae and
127 Typha. An overview of pollen taxa with abundances >1% for core LH 12-03 is plotted using Tilia
128 program (Grimm, 1993) in Figure 3. The pollen zonation was delimited visually by a cluster analysis of
129 taxa abundance >1% using CONISS (Grimm, 1987) (Fig. 3).

130 3.3. Geochemical analyses

131 An X-Ray fluorescence (XRF) Avaatech core scanner®, located at the University of Barcelona, was used
132 to measure light and heavy elements in the LH 12-03 core. An X-ray current of 650 μ A, a 10 second
133 count time and 10 kV X-ray voltage was used for measuring light elements, whereas 1700 μ A X-ray
134 current, 35 second count time and 30 kV X-ray voltage was used for heavy elements. Sampling interval
135 for these analyses was every 0.5 cm. For our study only three elements (K, Ca and Ti) have been
136 considered with enough counts to be representative.

137 Chemical composition was also determined on discrete samples every 2 cm. Prior to analysis, the samples
138 were dried in an oven and digested with HNO₃ and HF. Inductively coupled plasma-optical emission
139 spectrometry (ICP-OES; Perkin-Elmer optima 8300) was used for major element analysis. Blanks and
140 international standards were used for quality control – the analytical accuracy was higher than \pm 2.79%
141 and 1.89% for 50 ppm elemental concentrations of Al and Ca, respectively, and better than \pm 0.44% for 5
142 ppm elemental concentrations of K.

143 Trace element analysis was performed with an inductively coupled plasma mass spectrometry (ICP-MS;
144 Perkin Elmer Sciex Elan 5000). Samples were measured in triplicate through spectrometry using Re and
145 Rh as internal standards. The instrumental error is 2% for elemental concentrations of 50 ppm (Bea,
146 1996). All analyses were performed at the Instrumentations Center for Scientific Research (CIC),
147 University of Granada, Spain.

148 3.4. Mineralogical analyses

149 Morphological and compositional analyses were performed using scanning electron microscopy (SEM)
150 with an AURIGA model microscope (Carl Zeiss SMT) coupled with energy-dispersive X-ray



151 microanalysis (EDX) and Electron Backscatter Diffraction (EBSD) mode, also at the CIC (University of
152 Granada, Spain). Mineral grains were analysed to determine provenance, in particular those from eolian
153 origin.

154 3.5 Statistical Analysis

155 Principal components analysis (PCA) was run on the geochemical dataset using the PAST software
156 (Hammer et al., 2001). PCA finds hypothetical variables (components) accounting for as much as
157 possible of the variance in multivariate data (Davis, 1986; Harper, 1999). The elements used in the PCA
158 were standardized by subtracting the mean and dividing by the standard deviation (Davis, 1986). Pb was
159 not included in the PCA analysis due to its anthropogenic origin from mining and industrial pollution
160 during the latest Holocene in this area (García-Alix et al., 2013).

161 4. Results

162 4.1. Lithology and magnetic susceptibility

163 The LH 12-03 sediment core consists primarily of peat in the upper ~60 cm, with mostly sand and clay
164 layers below (Fig. 2). Positive MS peaks coincide with the grey clay intervals between 58-72 cm. Peat
165 intervals coincide with relatively low MS values. For example, a minimum in MS occurs at 36-48 cm
166 depth, related with a peaty interval with root remains. Near the bottom of the core, between 76-80 cm, a
167 sandy oxidized interval occurs.

168 4.2. Chronology and sedimentation rate

169 The age –model of LH 12-03 documents that the record spans the last 10800 cal yr BP (Table 1; Fig. 2).
170 Sediment accumulation rates (SAR) were calculated using the average rate from the Clam smooth spline
171 output (Fig. 2). The SAR below ~39 cm is very constant, varying between 0.049 and 0.061 mm yr⁻¹. The
172 SAR increases exponentially to 0.098 mm yr⁻¹ at 22 cm, 0.167 mm yr⁻¹ at ~9 cm and 0.357 mm yr⁻¹ at
173 the core top. Accordingly with the model age and the SAR, resolution of pollen analysis varies between
174 ~40 years per sample in the top of the core and ~120 years per sample in the lower part. The resolution of
175 the geochemical analysis on discrete samples changes between 100-400 years per sample, but the
176 geochemical XRF core scanning resolution ranges between 15-100 years per sample, providing higher
177 resolution than geochemical data on discrete sample. The MS analyses resolution varies between 15-
178 100 years per sample.

179 4.3. Pollen

180 Fifty distinct pollen taxa were recognized, but only those with abundance higher than 1% are included in
181 the pollen diagram (Fig. 3). Five pollen zones for the LH 12-03 record are identified, using variation in
182 pollen species plotted in Figure 3 and a cluster analysis run through the program CONISS (Grimm, 1987).
183 Zone LH-1 (core bottom-7000 cal yr BP) is defined by only three samples, due to the low preservation of
184 pollen in this interval. Pollen in this zone is dominated by an alternation between Asteraceae and *Pinus*
185 (Fig. 3). Arboreal pollen (AP), composed primarily of *Pinus*, but also *Quercus*, reaches its maximum



186 occurrence (90%) at ~7000 cal yr BP. The highest occurrence of Onagraceae pollen (~10%) takes place in
187 this zone, and Caryophyllaceae reaches high values during this zone (~10%) as well. Only minor
188 amounts of graminoids (Poaceae and Cyperaceae) occur during this period.

189 Zone LH-2 (~7000-4000 cal yr BP) is characterized by high percentages of tree species, primarily *Pinus*,
190 at the beginning of the zone (~90%), decreasing to ~55% at the upper part of the zone, with a minimum
191 (~30%) at 5000 cal yr BP. *Quercus* increases from ~2% at the beginning of the zone to ~10% at the end.
192 The highest percentages of *Betula* pollen (~5%) in the record occurs at this time. Asteraceae pollen (~5-
193 30%) is less than in LH-1, but Poaceae increases from <5% at the opening of the zone to >25%.
194 Caryophyllaceae and Onagraceae continue to show relatively high values in this zone (~5% and ~6%,
195 respectively). Cyperaceae occurs in high percentages (15%).

196 Zone LH-3 (~ 4000-2600 cal yr BP) is defined primarily by a great increase in Poaceae pollen (to ~60%)
197 (Fig. 3). Other important herbs and shrubs include Asteraceae (5-15%) and Caryophyllaceae (~5%).
198 Other pollen types that increase for the first time in this zone include Ericaceae (~3%), *Artemisia* (~3%)
199 and Ranunculaceae (~2-6%). *Pinus* (~3-25%) and Cyperaceae (0-14%) record a minimum in this zone,
200 and Onagraceae disappears altogether (Fig. 3).

201 Zone LH-4 (~ 2600-1450 cal yr BP) pollen assemblages show high variability in this zone. *Pinus* varies
202 between ~80% to ~3% from the onset to the end of the zone. Aquatic pollen such as Cyperaceae (~15%)
203 increases. On the other hand, an increase in herbs as Asteraceae (~5-70%) occurs along the zone, Poaceae
204 varies between ~7-12%.

205 Zone LH-5 (~ 1450-600 cal yr BP) is characterized by an increase in herbaceous pollen, led by Poaceae
206 (~35% maximum during this zone), Asteraceae (~60% maximum during this zone after ~1000 cal yr BP)
207 and *Artemisia* (~10%), and with the resulting decrease in AP. Since this zone to the present *Quercus* is
208 the major component of AP instead of *Pinus*. Cyperaceae also shows a decrease, and Ranunculaceae
209 reaches ~ 5%.

210 Zone LH-6 (~ 600 cal yr BP-present) is divided in two subzones. LH-6A (~ 600- 150 cal yr BP)
211 documents an increase in *Olea* (~6%), Poaceae (20%), Caryophyllaceae (7%) and *Artemisia* (~2-20%).
212 *Pinus* (~2%) and Asteraceae (~60%) decrease in this period. Aquatic and wetland pollen show a rise
213 (Cyperaceae ~30%, Ranunculaceae ~10%). LH-6B (~ 150 cal yr BP-present) depicts a further increase
214 in *Olea* (~25%), Poaceae (~40%) and *Artemisia* (~10%).

215 4.4. Sediment composition

216 Results of the geochemistry are described following the pollen zonation previously defined (see above).
217 The XRF-scanning method relies on determining the relative variations in elements. Nevertheless the
218 presence of major variations in organic matter or carbonates makes it important to normalize the
219 measured count in order to obtain an environmentally relevant signal (Lövemark et al., 2011).
220 Aluminium and titanium normalizations are commonly used to discern possible fluctuations in the
221 lithogenic fraction (enrichment or depletion of specific elements), particularly in the terrigenous
222 aluminosilicate sediment fraction (Van der Weijden, 2002; Calvert and Pedersen 2007; Martinez-Ruiz et
223 al., 2015). For this study, the XRF data were normalized to Ti since Al counts obtained were very low.
224 Poor detection of Al can be related to either low Al content, or high organic and water content that



225 increase radiation absorption and affect the intensity of this light element, among other possibilities
226 (Tjallingii et al., 2007).

227 Since data spacing is different between the analyses on discrete samples and the XRF scanner, a linear
228 interpolation was performed with the purpose of equalizing the space of the different time series (150-300
229 years). Afterwards, the mobile average was worked out along the time series (taking into account the 5
230 nearest points) in order to easily identify trends by means of smoothing out data irregularities. The
231 obtained data were compared, and both XRF-scanner and discrete sample data showed a good correlation.
232 As a consequence, the geochemical proxies displayed higher time resolution than the discrete samples
233 (Table 2). Discrete sample and XRF data results are described together in order to simplify this section
234 (Fig. 4).

235 Zone LH-1 (core bottom- ~7000 cal yr BP) is typified by maximum values of K/Al and K/Ti ratios,
236 coinciding with the lowest values in Ca/Al, Ca/Ti and Zr/Al ratios. Pb/Al data show a stable pattern
237 during this interval. Nevertheless, between 10000-9000 cal yr BP and ~8200 cal yr BP the trends were
238 reversed, with relatively low K/Al, low K/Ti and slightly increasing Zr/Al, Ca/Al and Ca/Ti ratios. A
239 positive peak in Pb/Al ratio at ~8200 cal yr BP is also observed.

240 Zone LH-2 (~7000-4000 cal yr BP) shows a decreasing trend in K/Al and K/Ti ratios, while an increasing
241 trend in Zr/Al, Ca/Al and Ca/Ti occurred. The Pb/Al ratio remains constant throughout this zone.

242 Zone LH-3 (~4000-2600 cal yr BP) documents an increase in Zr/Al, Ca/Al and Ca/Ti ratios, which
243 reaches a maximum at ~2600 cal yr BP. A K/Al and K/Ti minima occurs between ~3000 and ~2600 cal
244 yr BP. The Pb/Al ratio shows a positive peak at ~2800 cal yr BP.

245 Zone LH-4 (~2600-1450 cal yr BP) is characterized by low Ca/Al, Ca/Ti and Zr/Al ratios, with relatively
246 high K/Al and K/Ti ratios. The Pb/Al ratio shows a flat pattern, increasing at ~1500 cal yr BP.

247 Zone LH-5 (~1450- 650 cal yr BP) depicts higher ratios of Zr/Al, Ca/Al and Ca/Ti and decreasing ratios
248 of K/Al and K/Ti. A somewhat higher Pb/Al ratio is also registered during this period.

249 Zone LH-G6 (~ 650 cal yr BP- present) is divided in two subzones. During the LH-G6a subzone, low
250 values of Zr/Al and Ca/Ti ratios and minimum values Ca/Al ratio occur. Higher K/Al and K/Ti values are
251 also observed. The Pb/Al ratio decreases during this interval. LH-G6b is characterized by Zr/Al, Ca/Al,
252 Ca/Ti, K/Ti and Pb/Al maxima. Lower K/Al ratio occurs in this zone.

253 Several studies have demonstrated that PCA analysis of geochemical data can elucidate the importance of
254 different geochemical components driving the environmental responses in marine and lacustrine records
255 (Bahr et al., 2014; Yuan, 2017). We performed a PCA analysis of the LH geochemical data, which
256 yielded two significant components (Fig. 5). The first principal component (PC1) describes 58% of the
257 total variance. The main negative loadings for PC1 are Rb, Ba, Al, K, Ca, Mg and Sr, while large positive
258 loadings correspond to Zr and Rare Earth Elements (REE). The second principal component (PC2)
259 explains 17% of the total variance. The main negative loading for PC2 are Fe, Ca, Zr, Mg and Lu.
260 Positive loads correspond to Al, K, Ba, Sr and other elements.

261 SEM analyses show an alternation between a lithology rich in rock fragments and another rich in organic
262 remains. Also, diatom frustules, rich in silica, are particularly abundant since ~6300 cal yr BP to Present.
263 Other minerals such as zircon, rounded quartz and monazite were also identified (Fig.6).



264 5. Discussion

265 Pollen and geochemical proxies have been widely used for reconstructing vegetation changes and
266 environmental and climate variations in southern Iberia (e.g. Carrión, 2002; Sánchez-Goñi and Fletcher,
267 2008; Anderson et al., 2011; Nieto-Moreno et al., 2011; Jiménez-Moreno et al., 2012; Moreno et al.,
268 2012; Fletcher and Zielhofer, 2013; Jiménez-Espejo et al., 2014; Ramos-Román et al., 2016). Variations
269 in the occurrences of arboreal taxa such as *Pinus* and other mesic species (e.g. *Betula*, *Quercus*),
270 indicating relative humid and warm conditions, and xerophytic species (e.g., Poaceae, Asteraceae,
271 Amaranthaceae, *Artemisia*), representing aridity, have been useful for reconstructing relative humidity
272 changes in southern Iberian (e.g. Carrión et al., 2001, 2007, 2010; Anderson et al., 2011; Jiménez-Moreno
273 et al., 2012, 2013, 2015; Ramos-Román et al., 2016).

274 Over 75% of the total geochemical data variance is explained by the PC1 and PC2 (Fig. 5). We interpret
275 the results of PC1 as resulting from certain sorting between heavy minerals (positive loading; Zr and
276 REE) vs. clay minerals and feldspars (negative loadings; K, Al and Ca). The drainage basin is composed
277 mainly by mica schist, consequently enhanced in K-rich minerals such as mica and feldspar (Díaz de
278 Federico et al., 1980). PC1 points to a sorting between heavy minerals (enriched in Zr and REE) and clays
279 and feldspars (enriched in K and Al) (Fig. 5a), probably linked to physical weathering within the basin
280 and to resulting runoff until final deposition in the lake.

281 On the other hand, we interpret the results of PC2 as differentiating autochthonous elements (positive
282 loadings) vs. Saharan allochthonous input (negative loadings). In the first case, due to the abundance of
283 mica schist within the LH drainage basin (Díaz de Federico et al., 1980), the K/Al and K/Ti ratios are
284 interpreted as detrital products, and thus a proxy of runoff. In the second case, PC2 negative loading Zr,
285 Ca, Mg and Fe (Fig. 5b) grouped elements that are coherent with Saharan input composition (dolomite,
286 iron oxides and heavy minerals) (Ávila, 1997; Morales-Baquero et al., 2006b; Pulido-Villena et al.,
287 2007). In addition, Ca shows a strong positive correlation with Zr since 6300 cal yr BP ($r=0.57$; $p<0.05$)
288 supporting an eolian origin of the Ca in LH sediments. For instance, enrichment in heavy minerals such
289 as zircon and palygorskite has previously been used as an eolian proxy in the western Mediterranean (e.g.,
290 Combourieu Nebout et al., 2002, Rodrigo-Gámiz et al., 2011, 2015). High concentrations of Ca in other
291 lacustrine systems is usually associated with biogenic sources when anti-correlated with terrigenous
292 elements (Yuan, 2017). Nevertheless, elevated Ca in the LH record is linked with detrital elements, as
293 shown by PC1, where Ca is associated with K and Al (Fig. 5a). For these reasons Ca/Al and Ca/Ti ratios
294 are used in LH as eolian input proxies.

295 Elemental ratio variations, such as the ratios K/Al and K/Ti indicating fluvial input and ratios Zr/Al or
296 Zr/Th indicating aridity and eolian input, have been previously interpreted from Alboran Sea records as
297 well as in southern Iberia (Martín-Puertas et al., 2010; Nieto-Moreno et al., 2011, 2015; Rodrigo-Gámiz
298 et al., 2011; Jiménez-Espejo et al., 2014; Martínez-Ruiz et al., 2015; García-Alix et al., 2017). Thus, the
299 integration of both palynological data and geochemical ratios used as detrital input from LH have allowed
300 the reconstruction of the palaeoclimate and palaeoenvironmental history in Sierra Nevada during the
301 Holocene.

302 5.1. Holocene palaeoclimate and palaeoenvironmental history



303 5.1.1. Early and Mid-Holocene humid conditions (core bottom – ~7000 cal yr BP)

304 The wettest conditions are recorded during the Early Holocene in Sierra Nevada. This is shown in the LH
305 record by the highest K/Al ratio and MS values, and the low values in Zr/Al, Ca/Al and Ca/Ti ratios,
306 suggesting that runoff dominated over eolian processes at this time (zone LH-1; Fig. 7) and agrees with
307 previous studies in the area (Anderson et al., 2011; Jiménez-Moreno and Anderson, 2012; García-Alix et
308 al., 2012; Jiménez-Espejo et al., 2014). Unfortunately, the pollen record from LH during this interval is
309 insufficient to definitely confirm this interpretation, due to the high detrital sediment composition and low
310 organic content, as shown by the low MS values and low pollen preservation. However, high percentages
311 of AP in two out of three analysed samples suggest humid conditions and high runoff during this period.

312 An Early Holocene humid stage is noticed in other nearby sites, such as the south-faced Laguna de Río
313 Seco (LdRS; Fig. 1) (Anderson et al., 2011), when the highest lake level of the Holocene occurred. This is
314 also coeval with the dominance of arboreal species such as *Pinus* as well as aquatic and wetland plants
315 (Anderson et al., 2011). Low eolian input, noted by geochemical ratios, is also recorded in LdRS during
316 this interval (Jiménez-Espejo et al., 2014). Further indications of elevated humidity come from the north-
317 facing Borreguil de la Virgen (BdlV) (see Fig. 1), which is dominated by an AP assemblage and a high
318 occurrence of aquatic algae *Pediastrum* along with a higher lake level (Jiménez-Moreno et al., 2012).

319 Although the preponderance of evidence accumulated for the Early Holocene suggests overall humid
320 conditions, at least three relatively arid periods are identified with the geochemical data in the LH record
321 (Fig. 7). The first arid period occurred between ~9600-9000 cal yr BP, the second occurred ~8200 cal yr
322 BP and the third around 7500 cal yr BP.

323 The first arid event is characterized in LH by a decrease in K/Al and K/Ti ratios and MS, resulting from
324 the lower runoff input with the concomitant change to a more peaty composition. This event could be
325 correlated with a dryness event recorded in the Siles Lake record (Carrion, 2002) at ~9300 cal yr BP
326 noticed by an increase in *Pseudoschizaea*, which was coeval with a minor decrease in arboreal pollen also
327 recorded in several sites in North Iberia (Iriarte-Chiapusso et al., 2016). At marine site ODP 976 (Fig.1;
328 Combourieu-Nebout et al., 2009) a decrease in deciduous *Quercus* occurred between 9500-9200 cal yr
329 BP indicating a rapid excursion towards arid conditions (Fig.7). The speleothem record of Corchia Cave
330 also shows dryer conditions during this interval (Fig. 7; Regattieri et al., 2014) In addition, a decrease in
331 fluvial input in the Southern Alps and an aridification phase in southeastern France and southeastern
332 Iberia has been similarly recorded (Jalut et al., 2000).

333 The second dry event recorded at ~8200 cal yr BP is depicted in LH record by a negative peak in K/Ti
334 and K/Al ratios, and by the onset of a trend toward peatier lithology as evidenced by the MS profile. This
335 event is not recognized in LH record as clearly as the 9500 cal yr BP and the 7500 cal yr BP dry events. A
336 decrease in *Pinus* percentage is observed in the nearby LdRS (Anderson et al., 2011), while a forest
337 decrease is recorded in the Alboran Sea sites MD95-2043 and ODP 976. In several records from north
338 western Iberia a decrease in arboreal pollen also occurred at this time (Iriarte-Chiapusso et al., 2016).

339 The 8.2 ka event was the most rapid climate change towards cooler conditions occurred during the
340 Holocene. It was defined in Greenland ice cores by minimum values in $\delta^{18}\text{O}$ and affected the North
341 Atlantic basin and the Mediterranean area (Alley et al., 1997; Rasmussen et al., 2007; Wiersma et al.,
342 2011). Recent simulations point to a fresh water input in North Atlantic which could slow down the North



343 Atlantic Deep Water (NADW) formation preventing the heat transport over the north hemisphere
344 (Wiersma et al., 2010, 2011; Young et al., 2013).
345 Another dry event is recorded in LH at ~7500 cal yr BP evidenced by the higher peat content in the
346 sediment, as well as by the lower MS values and a relative minimum in the K/Ti ratio. A relative AP
347 minimum also occurred in LH at this time. This short-live event are depicted sharper than 8200 cal yr BP
348 event in several sites in southern Iberia and Alboran Sea: In the Padul record, located at 744 masl at the
349 lower part of Sierra Nevada a decrease in both evergreen and deciduous *Quercus* is interpreted as a dry
350 and cold event (Ramos-Román et al., in review); forest expansion in Guadiana valley during the early-
351 mid Holocene is interrupted by a xeric shrublands development between 7850-7390 cal yr BP (Fletcher et
352 al., 2007); in the Alboran Sea a decrease in deciduous *Quercus* is registered at site MD95-2043; at site
353 300G a decrease in winter and summer temperatures is also recorded during this interval (Jiménez-Espejo
354 et al., 2008); in lake Pergusa (south Italy) a trend toward arid conditions began at ~7500 cal yr BP
355 (Magny et al., 2012); in Corchia Cave an arid excursion occurred at ~7500 cal yr BP within an overall
356 humid period between 8300 cal yr BP and 7200 cal yr BP (Fig. 7; Regattieri et al., 2014).
357 Importantly, these arid events recorded in LH at 9600-9000 cal yr BP and 8200 cal yr BP are coeval with
358 the ice-rafted debris events 6 and 5 defined by Bond et al. 1997 in North Atlantic.

359 5.1.2. Mid- and Late Holocene (~7000 cal yr BP-2600 cal yr BP)

360 The Middle and Late Holocene in the southern Iberian Peninsula is characterized by a trend towards more
361 arid conditions (Jalut et al., 2009; Anderson et al., 2011; Rodrigo-Gámiz et al., 2011; Jiménez-Moreno
362 and Anderson, 2012; Jiménez-Espejo et al., 2014). In the LH record an abrupt decrease in the MS values
363 indicates a lithological change to more peaty sedimentation at ~7000 cal yr BP. Similarly, a decrease in
364 the K/Al and K/Ti ratios, points to a transition to less humidity and runoff (Fig. 7). *Quercus* percentages
365 increase at this time, partially replacing the *Pinus* which mainly compose the AP during the record. A
366 progressive increasing trend in eolian input from Sahara (Zr/Al, Ca/Al and Ca/Ti ratios) is observed
367 around 5500-6500 cal yr BP (Fig. 7), also pointing to an increase in aridity in the area. This change
368 coincides with regional increases in the Zr/Th ratio (equivalent to Zr/Al ratio) and *Artemisia* pollen, and
369 with decreases in *Betula* and *Pinus* in the LdRS record (Anderson et al., 2011; Jiménez-Espejo et al.,
370 2014), and in *Pinus* in the BdIV record (Jiménez-Moreno et al., 2012). Rodrigo-Gámiz et al. (2011) and
371 Jiménez-Espejo et al. (2014) observed similar geochemical patterns in western Mediterranean marine
372 records and in LdRS, with a decline in fluvial input, and a decline in surface runoff, respectively. The
373 same pattern is noticed in marine pollen records MD95-2043 and ODP 976 (Fletcher and Sanchez-Goñi,
374 2008; Combourieu-Nebout et al., 2009; Fig. 7). Contemporaneously, aridity is also suggested from
375 speleothem data around the Mediterranean area: At El Refugio cave, a hiatus in the speleothem growing
376 rate occurred between 7300-6100 cal year BP (Walczak et al., 2015), which is coeval with a drop in $\delta^{18}O$
377 in Soreq (Israel) and Corchia (Italy; CC26; Fig. 1 and 7) caves at 7000 cal yr BP (Bar-Matthews et al.,
378 2000; Zanchetta et al., 2007; Regattieri et al., 2014). Also at ~7000 cal yr BP a decreasing trend in the
379 deciduous/sclerophyllous pollen ratio occurred in southeastern France and Iberia (Jalut et al., 2000) and at
380 continental sites around the Mediterranean Sea (Jalut et al., 2009). In addition, very low lake levels were
381 recorded in the Sahara-Sahel Belt (Liu et al., 2007) and in the Southern Alps (Magny et al., 2002).



382 Enhanced arid conditions are observed in the LH record between 4000-2500 cal yr BP, interpreted
383 through a decline in AP, a Poaceae maximum and a peak in *Artemisia*. Also a surface runoff minimum
384 and an increase in eolian input proxies took place between 3500-2500 cal yr BP (zone LH-3). In Corchia
385 Cave an arid interval was recorded at ~3100 cal yr BP (Regattieri et al., 2014), coeval with another one
386 observed globally and described by Mayewski et al. (2004) between 3500-2500 cal yr BP. Nevertheless,
387 this period is not climatically stable, fluctuations are observed in in K/Ti, K/Al, Ca/Ti, Ca/Al and Zr/Al
388 ratios. Furthermore, peaks in *Quercus* are recorded in LH, LdlM and ODP 976 sites at ~3900 cal yr BP
389 and ~3100 cal yr BP, when AP in LH decreases (Combourieu-Nebout et al., 2009; Jiménez-Moreno et al.,
390 2013). This fact a priori contradictory, could be explained by altitudinal displacements of the tree taxa
391 such as *Quercus* in the oromediterranean belt due to the climatic variability occurred along this interval
392 (Carrión, 2002). During warmer periods, this species would be displaced towards higher elevation and the
393 influence of *Quercus* pollen in Sierra Nevada would be larger, this could explain relative
394 higher *Quercus* percentages in LdlM, LH and also in the ODP 976 record. The same relationship
395 between *Quercus* and *Pinus* is observed comparing the BdlC and Padul records, located closely but with
396 large altitude difference (BdlC ~2992 masl; Padul ~725 masl; Ramos-Román, 2018) where is also likely
397 linked to movements in the oromediterranean belt (Ramos-Román, 2018). These altitudinal displacements
398 of the tree taxa have been previously related to temperature changes in others southern Iberian records,
399 suggesting an ecological niche competition between *Pinus* and *Quercus* species at middle altitudes (see
400 Carrión et al., 2002 for a revision).

401 **5.1.3. Iberian Roman Humid Period (IRHP; ~2600-1450 cal yr BP)**

402 Because there is no consensus in the literature about the chronology for the main climatic stages during
403 the last 2000 years (Muñoz-Sobrino et al., 2014; Helama et al., 2017), here we follow the chronology
404 proposed by Moreno et al. (2012): Dark Ages (DA, 1450-1050 cal yr BP); Medieval Climate Anomaly
405 (MCA, 1050-650 cal yr BP); and LIA (650-100 cal yr BP). Another climatic stage precedes the DA – the
406 Iberian Roman Humid Period (IRHP, 2600-1600 cal yr BP), originally described by Martín-Puertas et al.
407 (2008). However, in the LH record we have established different IRHP limits (2600-1450), based
408 accordingly to the pollen zonation (Fig. 3), and coinciding with the DA onset defined by Moreno et al,
409 (2012).

410 The IRHP has been described as the wettest period in the western Mediterranean from proxies determined
411 both in marine and lacustrine records during the Late Holocene (Reed et al., 2001; Fletcher and Sanchez-
412 Goñi 2008; Combourieu-Nebout et al., 2009; Martín-Puertas et al., 2009; Nieto-Moreno et al., 2013;
413 Sánchez-López et al., 2016). A relative maximum in AP occurred in the LH record during this time, also
414 indicating forest development and relative high humidity during the Late Holocene in the area (zone LH-
415 4; Fig. 7). This is further supported by high K/Al and K/Ti ratios and MS values, indicating high detrital
416 input in the drainage basin, a minimum in Poaceae and low Saharan eolian input (low Ca/Al, Ca/Ti and
417 Zr/Al ratios) (Fig. 7). Fluvial elemental ratios have also shown an increase in river runoff in Alboran Sea
418 marine records (Nieto-Moreno et al., 2011; Rodrigo-Gámiz et al., 2011). This humid period seems to be
419 correlated with a solar maximum (Solanki et al., 2004) and persistent negative NAO conditions (Olsen et
420 al., 2012), which could have triggered general humid conditions in the Mediterranean. However, in the
421 LH record a decrease in AP between 2300-1800 occurred, pointing to arid conditions at that time. This



422 arid event also seems to show up in BdlC, with a decrease in AP between 2400-1900 cal yr BP (Ramos-
423 Román et al., 2016) and in Zoñar Lake, with water highly chemically concentrated and gypsum
424 deposition between 2140-1800 cal yr BP (Martín-Puertas et al., 2009). In Corchia Cave a rapid excursion
425 towards arid condition is recoded at ~2000 cal yr BP (Regattieri et al., 2014) (Fig.7).

426 **5.1.4. Dark Ages and Medieval Climate Anomaly (DA, MCA; 1450-650 cal yr BP)**

427 Predominantly arid conditions, depicted by high abundance of herbaceous and xerophytic species and an
428 AP minimum in the LH record, are shown for both DA and MCA (zone LH-5; Fig. 7). This is further
429 supported in this record by an increase in Saharan eolian input Ca/Al, Ca/Ti and Zr/Al ratios, and by a
430 decrease in surface runoff, indicated by the K/Al and K/Ti ratios (zone LH-5; Fig. 7). These results from
431 LH agree with climate estimations of overall aridity modulated by a persistent positive NAO phase during
432 this period (Trouet et al., 2009; Olsen et al., 2012), also previously noted by Ramos-Román et al. (2016)
433 in the area (Fig. 7).

434 Generally arid climate conditions during the DA and the MCA have also been previously described in the
435 LdlM and BdlC records, shown by a decrease in mesophytes and a rise of xerophytic vegetation during
436 that time (Jiménez-Moreno et al., 2013; Ramos-Román et al., 2016). Several pollen records in south and
437 central Iberian Peninsula also indicate aridity during the DA and MCA, for example grassland expanded
438 at Cañada de la Cruz, while in Siles Lake a lower occurrence of woodlands occurred (Carrión, 2002).
439 Also in Cimera Lake low lake level and higher occurrence of xerophytes were recorded (Sánchez-López
440 et al., 2016). Arid conditions were depicted in Zoñar Lake by an increase in *Pistacia* and heliophytes (i.e.,
441 Chenopodiaceae) and lower lake level (Martín-Puertas et al., 2010). Similar climatic conditions were
442 noticed in the marine records MD95-2043 and ODP 976 in the Alboran Sea through decreases in forest
443 (Fletcher and Sánchez-Goñi, 2008; Combourieu-Nebout et al., 2009; Fig. 7). Arid conditions in Basa de
444 la Mora (northern Iberian Peninsula) occurred during this time, characterized by maximum values of
445 *Artemisia*, and a lower development of deciduous *Quercus* and aquatic species such as *Potamogeton*, also
446 indicating low lake water levels (Moreno et al., 2012). Arid conditions were also documented by
447 geochemical data in marine records from the Alboran Sea (Nieto-Moreno et al., 2013, 2015), in the Gulf
448 of Lion and South of Sicily (Jalut et al., 2009). Aridity has also been interpreted for central Europe using
449 lake level reconstructions (Magny, 2004) and in speleothems records in central Italy (Regattieri et al.,
450 2014).

451 **5.1.5. Little Ice Age (LIA; 650-150 cal yr BP)**

452 The LIA is interpreted as an overall humid period in the LH record. This is indicated by higher AP values
453 than during the MCA, low Saharan dust input (low Ca/Al, Ca/Ti and Zr/Al ratios), a decrease in herbs
454 (Poaceae) and high values in the K/Al and K/Ti ratios indicating enhanced runoff (zone LH-6A; Fig. 7).
455 An increase in fluvial-derived proxies has been previously documented in other Iberian terrestrial records
456 such as Basa de la Mora Lake (Moreno et al., 2012), Zoñar Lake (Martín-Puertas et al., 2010) or Cimera
457 Lake (Sánchez-López et al., 2016) and marine records from the Alboran Sea basin (Nieto-Moreno et al.,
458 2011, 2015). Lake level reconstructions in Estanya Lake, in the Pre-Pyrenees (NE Spain), have shown
459 high water levels during this period (Morellón et al., 2009, 2011), supporting our humid climate



460 inferences. Nevertheless, recent high-resolution studies in Sierra Nevada (Ramos-Román et al., 2016;
461 García-Alix et al., 2017) and in several Iberian mountains (Oliva et al., 2018) have revealed that LIA was
462 not a climatically stable period and many oscillations at short-time scale occurred.

463 A persistently negative NAO phase, although with high variability, occurred during this time period
464 (Trouet et al., 2009), which could explain the overall humid conditions observed in southern Europe. As
465 in the Early Holocene arid events, solar variability has been hypothesized as the main forcing of this
466 climatic event (Bond et al., 2001; Mayewski et al., 2004; Fletcher et al., 2013; Ramos-Román et al.,
467 2016).

468 5.2. Anthropogenic impact in the southern Iberia

469 Previous studies, including the nearby LdRS record in Sierra Nevada, have shown that mining and
470 metallurgy activities commenced by ~4500 cal yr BP in this area (García-Alix et al., 2013, and references
471 therein), as shown by an enhanced Pb/Al ratio since this time. For the LH record, the first clear signal of
472 lead pollution from mining and smelting occurred around 2800 cal yr BP, coinciding with the Late
473 Bronze Age (LBA) (3200-2800 cal yr BP) and the Early Iron Age (EIA) (2800-2500 cal yr BP) (zone
474 LH-3; Fig. 8). The same signal is also recorded in the nearby LdRS (García-Alix et al., 2013; Fig 8).
475 Many studies, including LdRS, have shown that the IRHP was the most important lead pollution period
476 prior to the IP (Settle and Patterson, 1980). However, the Pb/Al record from LH does not register
477 enhanced pollution at this time. This could be due to a local effect, such as a higher catchment area in LH
478 involving a high runoff input, supported by an increase in the K/Al and K/Ti ratios during this humid
479 period that could have diluted the Pb signal transported by eolian input. Also a regional effect, such as a
480 weaker dust mobilization due to the humid conditions prevailing at this time, or patchy pollution
481 distribution, could explain these diverse records.

482 An increasing trend in *Artemisia*, which points to a climatic or anthropic aridification, is coeval with
483 another Pb/Al peak that occurred during the MCA (Fig. 8). Increasing anthropic activities during this time
484 in the area are justified by the first appearance of coprophilous fungi such as *Sordiales* and *Sporormiella*,
485 which occurred in BdIC (Ramos-Román et al., 2016) and in LdRS (Anderson et al., 2011), suggesting
486 grazing activity at high altitudes in Sierra Nevada (Anderson et al., 2011; Jiménez-Moreno and Anderson,
487 2012; Ramos-Román et al., 2016). Maxima in *Artemisia* and coprophilous fungi in Sierra Nevada are also
488 reached during the last 500 years (Anderson et al., 2011; Jiménez-Moreno and Anderson, 2012; Ramos-
489 Román et al., 2016).

490 An increase in the Pb/Al ratio is recorded during the IP in the LH record (Fig. 8), suggesting more
491 mining, fossil fuel burning or other human industrial activities. This is coeval with a rise in AP, which is
492 also related to human activities such as *Olea* commercial cultivation at lower elevations around Sierra
493 Nevada or *Pinus* reforestation in the area (Valbuena-Carabaña et al., 2010; Anderson et al., 2011). The
494 same pattern has also been observed in others records from Sierra Nevada (Jiménez-Moreno and
495 Anderson, 2012; García-Alix et al., 2013; Ramos-Román et al., 2016), in Zoñar Lake and the Alboran Sea
496 records (Martín-Puertas et al., 2010). In addition, a progressively increasing trend in Zr/Al and Ca/Al
497 ratios is observed during the last two centuries, which could be related to increasing local aridity and/or
498 anthropogenic desertification, but also with a change in the origin and/or composition of the dust reaching



499 to the lake (Jiménez-Espejo et al., 2014), likely related to the beginning of extensive agriculture and the
500 concomitant desertification in the Sahel region (Mulitza et al., 2010).

501 Therefore, the human impact in LH is mostly remarkable during the last two millennia. The comparison
502 with nearby records such as LdRS has also revealed that high-mountain lakes are very sensitive to human
503 activities (Anderson et al., 2011).

504 **5.3 Significance of the eolian record from Laguna Hondera**

505 Saharan dust influence over current alpine lake ecosystems is widely known (Morales-Baquero et al.,
506 2006a, 2006b; Pulido-Villena et al., 2008b; Mladenov et al., 2011), nevertheless, none of the previous
507 record preserved the relationship between elements found in present-day Saharan dust. The most
508 representative elements of Saharan dust in LH record are Fe, Zr and Ca as shown by the PC2 loading
509 (Fig. 5), where Ca and Fe directly affect the alpine lake biogeochemistry in this region (Pulido-Villena et
510 al., 2006, 2008b). Zirconium is transported in heavy minerals in eolian dust (Govin et al., 2012) and has
511 largely been used in the Iberian Peninsula and the western Mediterranean as an indicator of eolian
512 Saharan input (Moreno et al., 2005; Nieto-Moreno et al., 2011; Rodrigo-Gámiz et al., 2011; Jiménez-
513 Espejo et al., 2014; Martínez-Ruiz et al., 2015, and references therein). High Zr content has also been
514 identified in present aerosols at high elevations in Sierra Nevada (García-Alix et al., 2017). Considering
515 the low weatherable base cation reserves in LH bedrock catchment area, calcium is suggested to be
516 carried by atmospheric input of Saharan dust into alpine lakes in Sierra Nevada (Pulido-Villena et al.,
517 2006, see discussion; Morales-Baquero et al., 2013). This is the first time that the Ca signal is properly
518 recorded in a long record from Sierra Nevada. This could be explained by higher evaporation rates at this
519 site promoting annual lake desiccation that could prevent Ca water column dissolution and
520 using/recycling by organism, preserving better the original eolian signal. These elements have an essential
521 role as nutrients becoming winnowed and recycled rapidly in the oligotrophic alpine lake ecosystem
522 (Morales-Baquero et al., 2006b). This phenomenon has also been observed in other high-elevation lakes
523 where the phytoplankton is supported by a small and continually recycled nutrient pool (e.g., Sawatzky et
524 al., 2006).

525 The SEM observations further confirm the presence of Saharan dust in the lake sediments from LH and
526 the occurrence of Zircon, the main source of eolian Zr, which is relatively abundant (Fig. 6a). Quartz with
527 rounded morphologies (eolian erosion) are also frequent (Fig. 6b) in the uppermost part of the record as
528 well as REE rich minerals, such as monazite, which is typical from the Saharan-Sahel Corridor area
529 (Moreno et al., 2006) (Fig. 6c). In addition, the fact that the highest correlation between Ca and Zr
530 occurred after ~6300 cal yr BP, ($r=0.57$ $p<0.005$) along with the SEM observation and the low
531 availability of Ca in these ecosystems, could suggest that the beginning of Saharan dust arrivals to the
532 lake including both elements took place at this time, giving rise to the present way of nutrient inputs in
533 these alpine lakes (Morales-Baquero et al., 2006b; Pulido-Villena et al., 2006). The onset of Saharan dust
534 input into southern Iberia occurred prior to the end of the African Humid Period (AHP; ~5500 cal yr BP;
535 deMenocal et al., 2000), as previously noticed in the nearby LdRS (Jiménez-Espejo et al., 2014) and in
536 Alboran Sea (Rodrigo-Gámiz et al., 2011). This could suggest a progressive climatic deterioration in



537 North Africa, which culminated with the AHP demise and the massive Saharan dust input recorded in all
538 records in Sierra Nevada at ~3500 cal yr BP (Fig. 7).

539 6. Conclusions

540 The multiproxy paleoclimate analysis from LH has allowed the reconstruction of the vegetation and
541 climate evolution in Sierra Nevada and southern Iberia during the Holocene, and the possible factors that
542 have triggered paleoenvironmental changes. Climate during the Early Holocene was predominantly
543 humid, with two relatively arid periods between 10000-9000 and ~ 8200 cal yr BP, resulting in less
544 detrital inputs and a change to more peaty lithology. The onset of an arid trend took place around 7000
545 cal yr BP, decreasing the runoff input in the area. A significant increase in eolian-derived elements
546 occurred between 6300-5500 cal yr BP, coinciding with the AHP demise. An arid interval is recorded
547 between 4000-2500 cal yr BP, with a vegetation assemblage dominated by xerophytes.

548 Relative humid conditions occurred in the area between 2500-1450 cal yr BP, interrupting the Late
549 Holocene aridification trend. This humid interval was characterized by expansion of forest vegetation,
550 high runoff input, and a more clayey lithology. But during the DA and the MCA (1450-650 cal yr BP)
551 there was enhanced eolian input and an expansion of xerophytes, indicating increased arid conditions. In
552 contrast, the LIA (650-150 cal yr BP) was characterized by predominant humid conditions as pointed out
553 high runoff and low eolian input.

554 The first human impact signals in LH is recorded at ~2800 cal yr BP with a rise of Pb/Al ratio, coinciding
555 with the onset of mining in the Iberian Peninsula. The IP (150 cal yr BP-Present) is characterized in the
556 LH record by the highest values of the Pb/Al ratio, indicating fossil fuel burning by metallurgy industry,
557 enhanced of mining and other human activities.

558 Importantly, the LH record shows a unique and exceptional Ca signal derived from eolian input (high Ca-
559 Zr correlation) during the past ~6300 years in Sierra Nevada. The good preservation of the Ca record
560 might have been favoured by the high evaporation and the low lake depth that could have prevented Ca
561 column water dissolution and its re-use by organisms. Our record indicate that present-day inorganic
562 nutrient input from Sahara was established 6300 yrs ago and lasted until the present, with variations
563 depending on the prevailing climate.

564 Acknowledgements

565 This study was supported by the project P11-RNM 7332 of the “Junta de Andalucía”, the projects
566 CGL2013-47038-R, CGL2015-66830-R of the “Ministerio de Economía y Competitividad of Spain and
567 Fondo Europeo de Desarrollo Regional FEDER”, the research groups RNM0190 and RNM179 (Junta de
568 Andalucía). We also thank to Unidad de Excelencia (UCE-PP2016-05). J.M.M.F acknowledge the PhD
569 funding provided by Ministerio de Economía y Competitividad (CGL2015-66830-R) A.G.-A. was also
570 supported by a Marie Curie Intra-European Fellowship of the 7th Framework Programme for Research,
571 Technological Development and Demonstration of the European Commission (NAOSIPUK. Grant
572 Number: PIEF-GA-2012-623027) and by a Ramón y Cajal Fellowship RYC-2015-18966 of the Spanish
573 Government (Ministerio de Economía y Competitividad) and M.R.G. from the Andalucía Talent Hub
574 Program co-funded by the European Union’s Seventh Framework Program (COFUND – Grant



575 Agreement n° 291780) and the Junta de Andalucía. We thank Santiago Fernández, Maria Dolores
576 Hernandez and Antonio Mudarra for their help recovering the core and Inés Morales for the initial core
577 description and MS data. We thank Jaime Frigola (Universitat de Barcelona) for his help with XRF core
578 scanning.

579 **References**

580 Anderson, R. S., Jiménez-Moreno, G., Carrión, J. S., and Pérez-Martínez, C.: Holocene vegetation history
581 from Laguna de Río Seco, Sierra Nevada, southern Spain, *Quaternary Sci. Rev.* 30, 1615-1629,
582 DOI:10.1016/j.quascirev.2011.03.005, 2011.

583 Andrade, A., Valdeolillos, A., and Ruíz-Zapata, B.: Modern pollen spectra and contemporary
584 vegetation in the Paramera Mountain range (Ávila, Spain), *Rev. Palaeobot. Palyno.*, 82, 127-139,
585 DOI:10.1016/0034-6667(94)90024-8, 1994.

586 Ariztegui, D., Asioli, A., Lowe, J.J., Trincardi, F., Vigliotti, L., Tamburini, F., Chondrogianni, C.,
587 Accorsi, C.A., Bandini Mazzanti, M., Mercuri, A.M., Van der Kaars, S., McKenzie, J.A., and Oldfield,
588 F.: Palaeoclimate and the formation of sapropel S1: inferences from Late Quaternary lacustrine and
589 marine sequences in the central Mediterranean region, *Palaeogeogr. Palaeoclimatol.*, 158, 215-240,
590 DOI:10.1016/S0031-0182(00)00051-1, 2000.

591 Aubet, M.E.: *The Phoenicians and the West: Politics, colonies and trade*, Cambridge University Press,
592 Cambridge, 2001.

593 Ávila, A., Queralt-Mitjans, I., and Alarcón, M.: Mineralogical composition of African dust delivered by
594 red rains over northeastern Spain, *J. Geophys. Res.-Atmos.*, 102, 21977-21996, DOI:10.1029/97JD00485,
595 1997.

596 Ballantyne, A. P., Brahney, J., Fernandez, D., Lawrence, C. L., Saros, J., and Neff, J. C.: Biogeochemical
597 response of alpine lakes to a recent increase in dust deposition in the Southwestern US, *Biogeosciences*,
598 8, 2689, DOI:10.5194/bg-8-2689-2011, 2011.

599 Bar-Matthews, M., Ayalon, A., and Kaufman, A.: Timing and hydrological conditions of sapropel events
600 in the Eastern Mediterranean, as evident from speleothems, Soreq cave, Israel, *Chem. Geol.*, 169, 145-
601 156, DOI:10.1016/S0009-2541(99)00232-6, 2000.

602 Bahr, A., Jiménez-Espejo, F. J., Kolasinac, N., Grunert, P., Hernández-Molina, F. J., Röhl, U., Voelker,
603 A. H. L., Escutia, C., Stow, D. A. V., Hodell, D., and Alvarez-Zarikian, C. A.: Deciphering bottom
604 current velocity and paleoclimate signals from contourite deposits in the Gulf of Cádiz during the last 140
605 kyr: An inorganic geochemical approach, *Geochem. Geophys. Geosyst.*, 15, 3145-3160,
606 DOI:10.1002/2014GC005356, 2014.

607 Blaauw, M.: Methods and code for 'classical' age-modelling of radiocarbon sequences, *Quat.*
608 *Geochronol.*, 5, 512-518, DOI:10.1016/j.quageo.2010.01.002, 2010.



- 609 Bea, F.: Residence of REE, Y, Th and U in granites and crustal protoliths: implications for the chemistry
610 of crustal melts, *J. Petrol.*, 37, 521-532, DOI:10.1093/petrology/37.3.521, 1996.
- 611 Bond, G., Showers, W., Cheseby, M., Lotti, R., Almasi, P., deMenocal, P., Priore, P., Cullen, H., Hajdas,
612 I., and Bonani, G.: A pervasive millennial-scale cycle in North Atlantic Holocene and glacial climates,
613 *Science*, 278, 1257-1266, DOI:10.1126/science.278.5341.1257, 1997.
- 614 Bond, G., Kromer, B., Beer, J., Muscheler, R., Evans, M., Showers, W., Hoffmann, S., Lotti-Bond, R.,
615 Hajdas, I., and Bonani, G.: Persistent solar influence on North Atlantic climate during the Holocene,
616 *Science*, 294, 2130-2136, DOI:10.1126/science.1065680, 2001.
- 617 Cacho, I., Grimalt, J. O., and Canals, M.: Response of the Western Mediterranean Sea to rapid climatic
618 variability during the last 50,000 years: a molecular biomarker approach, *J. Marine Syst.*, 33-34, 253-272,
619 DOI:10.1016/S0924-7963(02)00061-1, 2002.
- 620 Calvert, S. E., and Pedersen, T. F.: Elemental proxies for palaeoclimatic and palaeoceanographic
621 variability in marine sediments: interpretation and application, *Proxies in Late Cenozoic*
622 *Paleoceanography*, Elsevier, Amsterdam, 2007.
- 623 Carrión, J. S.: Patterns and processes of Late Quaternary environmental change in a montane region of
624 southwestern Europe, *Quaternary Sci. Rev.*, 21, 2047-2066, DOI:10.1016/S0277-3791(02)00010-0, 2002.
- 625 Carrión, J. S., Munuera, M., Dupré, M., and Andrade, A.: Abrupt vegetation changes in the Segura
626 mountains of southern Spain throughout the Holocene, *J. Ecol.*, 89, 783-797, DOI:10.1046/j.0022-
627 0477.2001.00601.x, 2001.
- 628 Carrión, J.S., Sánchez-Gómez, P., Mota, J. F., Yll, E. I., and Chaín, C.: Fire and grazing are contingent on
629 the Holocene vegetation dynamics of Sierra de Gádor, southern Spain, *Holocene* 13, 839-849,
630 DOI:10.1191/0959683603hl662rp, 2003.
- 631 Carrión, J. S., Fuentes, N., González-Sampériz, P., Sánchez Quirante, L., Finlayson, J. C., Fernández, S.,
632 and Andrade, A.: Holocene environmental change in a montane region of southern Europe with a long
633 history of human settlement, *Quaternary Sci. Rev.*, 26, 1455-1475, DOI:10.1016/j.quascirev.2007.03.013,
634 2007.
- 635 Carrión, J. S., Fernández, S., González-Sampériz, P., Gil-Romera, G., Badal, E., Carrión-Marco, Y.,
636 López-Merino, L., López-Sáez, J. A., Fierro, E., and Burjachs, F.: Expected trends and surprises in the
637 Lateglacial and Holocene vegetation history of the Iberian Peninsula and Balearic Islands, *Rev.*
638 *Palaeobot. Palyno.*, 162, 458-476, DOI:10.1016/j.jaridenv.2008.11.014, 2010.
- 639 Castillo Martín, A.: *Lagunas de Sierra Nevada*, Universidad de Granada, Granada, 2009.
- 640 Combourieu Nebout, N., Turon, J. L., Zahn, R., Capotondi, L., Londeix, L., and Pahnke, K.: Enhanced
641 aridity and atmospheric high-pressure stability over the western Mediterranean during the North Atlantic
642 cold events of the past 50 ky, *Geology*, 30, 863-866, DOI:10.1130/0091-
643 7613(2002)030<0863:EAAAHP>2.0.CO;2, 2002..



- 644 Combourieu Nebout, N., Peyron, O., Dormoy, I., Desprat, S., Beaudouin, C., Kotthoff, U., and Marret, F.:
645 Rapid climatic variability in the west Mediterranean during the last 25,000 years from high resolution
646 pollen data, *Clim. Past*, 5, 503-521, DOI:10.5194/cpd-5-671-2009, 2009.
- 647 Comero, S., Locoro, G., Free, G., Vaccaro, S., De Capitani, L., and Gawlik, B. M.: Characterisation of
648 Alpine lake sediments using multivariate statistical techniques, *Chemometr. Intell. Lab.*, 107(1), 24-30,
649 DOI:10.1016/j.chemolab.2011.01.002, 2011.
- 650 Davis, J. C., and Sampson, R. J.: *Statistics and data analysis in geology*, Wiley, New York, 1986.
- 651 de Lange, G. J., Thomson, J., Reitz, A., Slomp, C. P., Principato, M. S., Erba, E., and Corselli, C.:
652 Synchronous basin-wide formation and redox-controlled preservation of a Mediterranean sapropel, *Nat.*
653 *Geosci.*, 1, 606-610, DOI:10.1038/ngeo283, 2008.
- 654 deMenocal, P., Ortiz, J., Guilderson, T., Adkins, J., Sarnthein, M., Baker, L., and Yarusinsky, M.: Abrupt
655 onset and termination of the African Humid Period: rapid climate responses to gradual insolation forcing,
656 *Quaternary Sci. Rev.*, 19, 347-361, DOI:10.1016/S0277-3791(99)00081-5, 2000.
- 657 Díaz de Federico, A.: *Estudio geológico del Complejo de Sierra Nevada en la transversal del Puerto de la*
658 *Ragua (Cordillera Bética)*, Ph.D. thesis, Universidad de Granada, Granada, 1980.
- 659 El Aallali, A., López Nieto, J. M., Pérez Raya, F., and Molero Mesa, J.: Estudio de la vegetación forestal
660 en la vertiente sur de Sierra Nevada (Alpujarra Alta granadina), *Itinera Geobot.*, 11, 387-402, 1998.
- 661 Faegri, K., and Iversen, J.: *Textbook of Pollen Analysis*, Wiley, New York, 1989.
- 662 Fletcher, W. J., Boski, T., and Moura, D.: Palynological evidence for environmental and climatic change
663 in the lower Guadiana valley, Portugal, during the last 13 000 years, *Holocene*, 17, 481-494,
664 DOI:10.1177/0959683607077027, 2007.
- 665 Fletcher, W. J., and Sánchez Goñi, M. F.: Orbital- and sub-orbital-scale climate impacts on vegetation of
666 the western Mediterranean basin over the last 48,000 yr, *Quaternary Res.*, 70, 451-464,
667 DOI:10.1016/j.yqres.2008.07.002, 2008.
- 668 Fletcher, W. J., Sánchez Goñi, M. F., Peyron, O., and Dormoy, I.: Abrupt climate changes of the last
669 deglaciation detected in a Western Mediterranean forest record, *Clim. Past*, 6, 245-264, DOI:10.5194/cp-
670 6-245-2010, 2010.
- 671 Fletcher, W. J., and Zielhofer, C.: Fragility of Western Mediterranean landscapes during Holocene rapid
672 climate changes, *Catena*, 103, 16-29, DOI:10.1016/j.catena.2011.05.001, 2013.
- 673 García-Alix, A., Jiménez-Moreno, G., Anderson, R. S., Jiménez-Espejo, F. J., and Delgado-Huertas, A.:
674 Holocene paleoenvironmental evolution of a high-elevation wetland in Sierra Nevada, southern Spain,
675 deduced from an isotopic record, *J. Paleolimnol.*, 48, 471-484, DOI:10.1007/s10933-012-9625-2, 2012.
- 676 García-Alix, A., Jiménez-Espejo, F. J., Lozano, J. A., Jiménez-Moreno, G., Martínez-Ruiz, F., García
677 Sanjuán, L., Aranda Jiménez, G., García Alfonso, E., Ruiz-Puertas, G., and Anderson, R. S.:
678 Anthropogenic impact and lead pollution throughout the Holocene in Southern Iberia, *Sci. Total Environ.*,
679 449, 451-460, DOI:10.1016/j.scitotenv.2013.01.081, 2013.



- 680 García-Alix, A., Jimenez Espejo, F. J., Toney, J. L., Jiménez-Moreno, G., Ramos-Román, M. J.,
681 Anderson, R.S., Ruano, P., Queralt, I., Delgado Huertas, A., and Kuroda, J.: Alpine bogs of southern
682 Spain show human-induced environmental change superimposed on long-term natural variations, *Sci.*
683 *Rep.-UK*, 7, 7439, DOI:10.1038/s41598-017-07854-w, 2017.
- 684 Govin, A., Holzwarth, U., Heslop, D., Ford Keeling, L., Zabel, M., Mulitza, S., Collins, J. A., and
685 Chiessi, C. M.: Distribution of major elements in Atlantic surface sediments (36°N-49°S): imprint of
686 terrigenous input and continental weathering, *Geochem. Geophys. Geosy.*, 13, Q01013,
687 DOI:10.1029/2011GC003785, 2012.
- 688 Grimm, E. C.: CONISS: a Fortran 77 program for stratigraphically constrained cluster analysis by the
689 method of incremental sum of squares, *Comput. Geosci.*, 13, 13-35, DOI:10.1016/0098-3004(87)90022-
690 7, 1987.
- 691 Grimm, E.: TILIA: a pollen program for analysis and display, Illinois State Museum, Springfield, 1993.
- 692 Hammer, Ø., Harper, D. A. T., and Ryan, P. D.: Paleontological Statistics Software Package for
693 Education and Data Analysis, *Palaeontol. electron.*, 4, 1-9, 2001.
- 694 Harper, D. A. T.: Numerical Palaeobiology, John Wiley & Sons, Chichester, 1999.
- 695 Helama, S., Jones, P. D., and Briffa, K. R.: Dark Ages Cold Period: A literature review and directions for
696 future research, *Holocene* 27, 1600-1606, DOI: 10.1177/0959683617693898, 2017.
- 697 Jalut, G., Esteban Amat, A., Bonnet, L., Gauquelin, T., and Fontugne, M.: Holocene climatic changes in
698 the Western Mediterranean, from south-east France to south-east Spain, *Palaeogeogr. Palaeoclimatol.*, 160, 255-
699 290, DOI:10.1016/S0031-0182(00)00075-4, 2000.
- 700 Jalut, G., Dedoubat, J. J., Fontugne, M., and Otto, T.: Holocene circum-Mediterranean vegetation
701 changes: climate forcing and human impact, *Quatern. Int.*, 200, 4-18, DOI:10.1016/j.quaint.2008.03.012,
702 2009.
- 703 Jiménez-Espejo, F. J., Martínez-Ruiz, F., Rogerson, M., González-Donoso, J. M., Romero, O., Linares,
704 D., Sakamoto, T., Gallego-Torres, D., Rueda Ruiz, J. L., Ortega-Huertas, M., and Perez Claros, J. A.:
705 Detrital input, productivity fluctuations, and water mass circulation in the westernmost Mediterranean Sea
706 since the Last Glacial Maximum, *Geochem. Geophys. Geosy.*, 9, Q11U02, DOI:10.1029/2008GC002096,
707 2008.
- 708 Jiménez-Espejo, F. J., García-Alix, A., Jiménez-Moreno, G., Rodrigo-Gámiz, M., Anderson, R. S.,
709 Rodríguez-Tovar, F. J., Martínez-Ruiz, F., Giral, S., Delgado-Huertas, A., and Pardo-Igúzquiza, E.:
710 Saharan aeolian input and effective humidity variations over western Europe during the Holocene from a
711 high altitude record, *Chem. Geol.*, 374, 1-12, DOI:10.1016/j.chemgeo.2014.03.001, 2014.
- 712 Jiménez-Moreno, G., and Anderson, R. S.: Holocene vegetation and climate change recorded in alpine
713 bog sediments from the Borreguiles de la Virgen, Sierra Nevada, southern Spain, *Quaternary Res.*, 77, 44-
714 53, DOI:10.1016/j.yqres.2011.09.006, 2012.



- 715 Jiménez-Moreno, G., García-Alix, A., Hernández-Corbalán, M. D., Anderson, R. S., and Delgado-
716 Huertas, A.: Vegetation, fire, climate and human disturbance history in the southwestern Mediterranean
717 area during the late Holocene, *Quaternary Res.*, 79, 110-122, DOI:10.1016/j.yqres.2012.11.008, 2013.
- 718 Jiménez-Moreno, G., Rodríguez-Ramírez, A., Pérez-Asensio, J. N., Carrión, J. S., López-Sáez, J. A.,
719 Villarías-Robles, J. J. R., Celestino-Pérez, S., Cerrillo-Cuenca, E., Ángel León, A., and Contreras, C.:
720 Impact of late-Holocene aridification trend, climate variability and geodynamic control on the
721 environment from a coastal area in SW Spain, *Holocene*, 25, 607-617, DOI:10.1177/0959683614565955,
722 2015.
- 723 Lionello, P., Malanotte-Rizzoli, P., Boscolo, R., Alpert, P., Artale, V., Li, L., Luterbacher, J., May, W.,
724 Trigo, R., Tsimplis, M., Ulbrich, U., and Xoplaki, E.: The Mediterranean climate: an overview of the
725 main characteristics and issues, *Developments in Earth and Environmental Sciences*, 4, Elsevier,
726 Amsterdam, Netherlands, 1-26, 2006.
- 727 Liu, Z., Wang, Y., Gallimore, R., Gasse, F., Johnson, T., deMenocal, P., Adkins, J., Notaro, M., Prentice,
728 I. C., Kutzbach, J., Jacob, R., Behling, P., Wang, L., and Ong, E.: Simulating the transient evolution and
729 abrupt change of Northern Africa atmosphere–ocean–terrestrial ecosystem in the Holocene. *Quaternary*
730 *Sci. Rev.*, 26, 1818-1837, DOI:10.1016/j.quascirev.2007.03.002, 2007.
- 731 Löwemark, L., Chen, H.-F., Yang, T.-N., Kylander, M., Yu, E.-F., Hsu, Y.-W., Lee, T.-Q., Song, S.-R.,
732 and Jarvis, S.: Normalizing XRF-scanner data: a cautionary note on the interpretation of high-resolution
733 records from organic-rich lakes, *J. Asian Earth Sci.*, 40, 1250-1256, DOI:10.1016/j.jseas.2010.06.002,
734 2011.
- 735 Magny, M., Miramont, C., and Sivan, O.: Assessment of the impact of climate and anthropogenic factors
736 on Holocene Mediterranean vegetation in Europe on the basis of palaeohydrological records,
737 *Palaeogeogr. Palaeoclimatol.*, 186, 47-59, DOI:10.1016/S0031-0182(02)00442-X, 2002.
- 738 Magny, M., and Bégeot, C.: Hydrological changes in the European midlatitudes associated with
739 freshwater outbursts from Lake Agassiz during the Younger Dryas event and the early Holocene,
740 *Quaternary Res.*, 61, 181-192, doi:10.1016/j.yqres.2003.12.003, 2004.
- 741 Magny, M., de Beaulieu, J.-L., Drescher-Schneider, R., Vannière, B., Walter-Simonnet, A.-V., Miras, Y.,
742 Millet, L., Bossuet, G., Peyron, O., Brugiapaglia, E., and Leroux, A.: Holocene climate changes in the
743 central Mediterranean as recorded by lake-level fluctuations at Lake Accesa (Tuscany, Italy), *Quaternary*
744 *Sci. Rev.*, 26, 1736-1758, DOI:10.1016/j.quascirev.2007.04.014, 2007.
- 745 Magny, M., Peyron, O., Sadori, L., Ortu, E., Zanchetta, G., Vannière, B., and Tinner, W.: Contrasting
746 patterns of precipitation seasonality during the Holocene in the south- and north- central Mediterranean.
747 *J. Quat. Sci.*, 27, 290-296, DOI:10.1002/jqs.1543, 2012.
- 748 Martín-Puertas, C., Valero-Garcés, B. L., Mata, M. P., González-Sampériz, P., Bao, R., Moreno, A., and
749 Stefanova, V.: Arid and humid phases in southern Spain during the last 4000 years: the Zonar Lake
750 record, *Cordoba, Holocene*, 18, 907-921, DOI:10.1177/0959683608093533, 2008.



- 751 Martín-Puertas, C., Valero-Garcés, B. L., Brauer, A., Mata, M. P., Delgado-Huertas, A., and Dulski, P.:
752 The Iberian–Roman Humid Period (2600–1600 cal yr BP) in the Zoñar Lake varve record (Andalucía,
753 southern Spain), *Quaternary Res.*, 71, 108-120, DOI:10.1016/j.yqres.2008.10.004, 2009.
- 754 Martín-Puertas, C., Jiménez-Espejo, F., Martínez-Ruiz, F., Nieto-Moreno, V., Rodrigo, M., Mata, M. P.,
755 and Valero-Garcés, B. L.: Late Holocene climate variability in the southwestern Mediterranean region: an
756 integrated marine and terrestrial geochemical approach, *Clim. Past*, 6, 807-816, DOI:10.5194/cp-6-807-
757 2010, 2010.
- 758 Martínez-Ruiz, F., Kastner, M., Gallego-Torres, D., Rodrigo-Gámiz, M., Nieto-Moreno, V., and Ortega-
759 Huertas, M.: Paleoclimate and paleoceanography over the past 20,000 yr in the Mediterranean Sea
760 Basins as indicated by sediment elemental proxies, *Quaternary Sci. Rev.*, 107, 25-46,
761 DOI:10.1016/j.quascirev.2014.09.018, 2015.
- 762 Mayewski, P. A., Rohling, E. E., Curt Stager, J., Karlén, W., Maasch, K. A., David Meeker, L.,
763 Meyerson, E. A., Gasse, F., van Kreveld, S., Holmgren, K., Lee-Thorp, J., Rosqvist, G., Rack, F.,
764 Staubwasser, M., Schneider, R. R., and Steig, E. J.: Holocene climate variability, *Quaternary Res.* 62,
765 243-255, DOI: 10.1016/j.yqres.2004.07.001, 2004.
- 766 Mladenov, N., Pulido-Villena, E., Morales-Baquero, R., Ortega-Retuerta, E., Sommaruga, R., and Reche,
767 I.: Spatiotemporal drivers of dissolved organic matter in high alpine lakes: Role of Saharan dust inputs
768 and bacterial activity, *J. Geophys. Res.-Biogeo.*, 113, DOI:10.1029/2008JG000699, 2008.
- 769 Mladenov, N., Sommaruga, R., Morales-Baquero, R., Laurion, I., Camarero, L., Diéguez, M.C., Camacho,
770 A., Delgado, A., Torres, O., Chen, Z., Felip, M., and Reche, I.: Dust inputs and bacteria influence
771 dissolved organic matter in clear alpine lakes, *Nat. Commun.* 2, 405, DOI:10.1038/ncomms1411, 2011.
- 772 Morales-Baquero, R., Carrillo, P., Reche, I., and Sánchez-Castillo, P.: Nitrogen-phosphorus relationship
773 in high mountain lakes: effects of the size of catchment basins, *Can. J. Fish. Aquat. Sci.*, 56, 1809-1817,
774 DOI:10.1139/cjfas-56-10-1809, 1999.
- 775 Morales-Baquero, R., Pulido-Villena, E., and Reche, I.: Atmospheric inputs of phosphorus and nitrogen
776 to the southwest Mediterranean region: Biogeochemical responses of high mountain lakes, *Limnol.*
777 *Oceanogr.*, 51, 830-837, DOI:10.4319/lo.2006.51.2.0830, 2006a.
- 778 Morales-Baquero R., Pulido-Villena E., Romera O., Ortega-Retuerta E., Conde-Porcuna J. M., Pérez-
779 Martínez C., and Reche I.: Significance of atmospheric deposition to freshwater ecosystems in the southern
780 Iberian Peninsula, *Limnetica*, 25, 171-180, 2006b.
- 781 Morales-Baquero, R., Pulido-Villena, E., and Reche, I.: Chemical signature of Saharan dust on dry and
782 wet atmospheric deposition in the south-western Mediterranean region, *Tellus B*, 65,
783 DOI:10.3402/tellusb.v65i0.18720, 2013.
- 784 Moreno, A., Pérez, A., Frigola, J., Nieto-Moreno, V., Rodrigo-Gámiz, M., Martrat, B., González-
785 Sampéris, P., Morellón, M., Martín-Puertas, C., Corella, J. P., Belmonte, A., Sancho, C., Cacho, I.,
786 Herrera, G., Canals, M., Grimalt, J. O., Jiménez-Espejo, F. J., Martínez-Ruiz, F., Vegas-Villarrúbia, T.,



- 787 and Valero-Garcés, B. L.: The Medieval Climate Anomaly in the Iberian Peninsula reconstructed from
788 marine and lake records, *Quaternary Sci. Rev.*, 42, 16-32, DOI:10.1016/j.quascirev.2012.04.007, 2012.
- 789 Moreno, T., Querol, X., Castillo, S., Alastuey, A., Cuevas, E., Herrmann, L., Mounkaila, M., Elvira, J.,
790 Gibbons, W.: Geochemical variations in aeolian mineral particles from the Sahara–Sahel Dust Corridor.
791 *Chemosphere*, 65, 261-270, DOI:10.1016/j.chemosphere.2006.02.052, 2006.
- 792 Morellón, M., Valero-Garcés, B., Vegas-Vilarrúbia, T., González-Sampérez, P., Romero, O., Delgado-
793 Huertas, A., Mata, P., Moreno, A., Rico, M., and Corella, J. P.: Lateglacial and Holocene
794 palaeohydrology in the western Mediterranean region: the Lake Estanya record (NE Spain), *Quaternary*
795 *Sci. Rev.*, 28, 2582-2599, DOI:10.1016/j.quascirev.2009.05.014, 2009.
- 796 Morellón, M., Valero-Garcés, B., González-Sampérez, P., Vegas-Vilarrúbia, T., Rubio, E., Rieradevall,
797 M., Delgado-Huertas, A., Mata, P., Romero, O., Engstrom, D. R., López-Vicente, M., Navas, A., and
798 Soto, J.: Climate changes and human activities recorded in the sediments of Lake Estanya (NE Spain)
799 during the Medieval Warm Period and Little Ice Age, *J. Paleolimnol.*, 46, 423-452, DOI:10.1007/s10933-
800 009-9346-3, 2011.
- 801 Mulitza, S., Heslop, D., Pittauerova, D., Fischer, H. W., Meyer, I., Stuut, J.-B., Zabel, M., Mollenhauer,
802 G., Collins, J.A., Kuhnert, H., and Schulz, M.: Increase in African dust flux at the onset of commercial
803 agriculture in the Sahel region, *Nature*, 466, 226-228, DOI:10.1038/nature09213, 2010.
- 804 Sobrino, C. M., García-Moreiras, I., Castro, Y., Carreño, N. M., de Blas, E., Rodríguez, C. F., Judd, A.,
805 and García-Gil, S., Climate and anthropogenic factors influencing an estuarine ecosystem from NW
806 Iberia: new high resolution multiproxy analyses from San Simón Bay (Ría de Vigo), *Quaternary Sci.*
807 *Rev.*, 93, 11-33, DOI:10.1016/j.quascirev.2014.03.021, 2014.
- 808 Nieto-Moreno, V., Martínez-Ruiz, F., Giralt, S., Jiménez-Espejo, F. J., Gallego-Torres, D., Rodrigo-
809 Gámiz, M., García-Orellana, J., Ortega-Huertas, M., and de Lange, G. J.: Tracking climate variability in
810 the western Mediterranean during the Late Holocene: a multiproxy approach, *Clim. Past*, 7, 1395-1414,
811 DOI:10.5194/cp-7-1395-2011, 2011.
- 812 Nieto-Moreno, V., Martínez-Ruiz, F., Willmott, V., García-Orellana, J., Masqué, P., and Damsté, J. S.:
813 Climate conditions in the westernmost Mediterranean over the last two millennia: An integrated
814 biomarker approach, *Org. Geochem.*, 55, 1-10. DOI:10.1177/0959683613484613, 2013
- 815 Nieto-Moreno, V., Martínez-Ruiz, F., Gallego-Torres, D., Giralt, S., García-Orellana, J., Masqué, P.,
816 Sinninghe Damsté, J.S., and Ortega-Huertas, M.: Palaeoclimate and palaeoceanographic conditions in the
817 westernmost Mediterranean over the last millennium: an integrated organic and inorganic approach, *J.*
818 *Geol. Soc. London*, 172, 264-271, DOI: 10.1144/jgs2013-105, 2015.
- 819 Oliva, M., Ruiz-Fernández, J., Barriendos, M., Benito, G., Cuadrat, J. M., Domínguez-Castro, F., García-
820 Ruiz, J. M., Giralt, S., Gómez-Ortiz, A., Hernández, A., López-Costas, O., López-Moreno, J. I., López-
821 Sáez, J. A., Matínez-Cortízar, A., Moreno, A., Prohom, M., Saz, M. A. Serrano, E., Tejedor, E., Trigo, R.,
822 Valero-Garcés, B. and López-Costas, O.: The Little Ice Age in Iberian mountains, *Earth-Sci. Rev.*, 177,
823 175-208, DOI:10.1016/j.earscirev.2017.11.010, 2018.



- 824 Olsen, J., Anderson, N. J., and Knudsen, M. F.: Variability of the North Atlantic Oscillation over the past
825 5,200 years, *Nat. Geosci.*, 5, 808-812, DOI:10.1038/ngeo1589, 2012.
- 826 Palma, P., Oliva, M., García-Hernández, C., Ortiz, A. G., Ruiz-Fernández, J., Salvador-Franch, F., and
827 Catarineu, M: Spatial characterization of glacial and periglacial landforms in the highlands of Sierra
828 Nevada (Spain). *Sci. Total Environ.*, 584, 1256-1267, DOI:10.1016/j.scitotenv.2017.01.196.
- 829 Pulido-Villena, E., Reche, I., and Morales-Baquero, R.: Significance of atmospheric inputs of calcium
830 over the southwestern Mediterranean region: High mountain lakes as tools for detection, *Global
831 Biogeochem. Cy.*, 20, GB2012, DOI:10.1029/2005GB002662, 2006.
- 832 Pulido-Villena, E., Wagener, T., and Guieu, C.: Bacterial response to dust pulses in the western
833 Mediterranean: Implications for carbon cycling in the oligotrophic ocean, *Global Biogeochem. Cy.*, 22,
834 DOI:10.1029/2007GB003091, 2008a.
- 835 Pulido-Villena, E., Reche, I., and Morales-Baquero, R.: Evidence of an atmospheric forcing on
836 bacterioplankton and phytoplankton dynamics in a high mountain lake, *Aquat. sci.*, 70, 1-9,
837 DOI:10.1007/s00027-007-0944-8, 2008b.
- 838 Ramos-Román, M. J., Jiménez-Moreno, G., Anderson, R. S., García-Alix, A., Toney, J. L., Jiménez-
839 Espejo, F. J., and Carrión, J. S.: Centennial-scale vegetation and North Atlantic Oscillation changes
840 during the Late Holocene in the southern Iberia, *Quaternary Sci. Rev.*, 143, 84-95,
841 DOI:10.1016/j.quascirev.2016.05.007, 2016.
- 842 Ramos-Román, M. J.: Holocene paleoenvironmental change, climate and human impact in Sierra Nevada,
843 Southern Iberian Peninsula, Ph. D. Thesis, Universidad de Granada, Granada, 2018.
- 844 Rasmussen, S. O., Vinther, B. M., Clausen, H. B., and Andersen, K. K.: Early Holocene climate
845 oscillations recorded in three Greenland ice cores, *Quaternary Sci. Rev.*, 26, 1907-1914,
846 DOI:10.1016/j.quascirev.2007.06.015, 2007.
- 847 Reche, I., Ortega-Retuerta, E., Romera, O., Villena, E. P., Baquero, R. M., and Casamayor, E. O.: Effect
848 of Saharan dust inputs on bacterial activity and community composition in Mediterranean lakes and
849 reservoirs, *Limnol. Oceanogr.*, 54, 869-879, DOI:10.4319/lo.2009.54.3.0869, 2009.
- 850 Reed, J. M., Stevenson, A. C., and Juggins, S.: A multi-proxy record of Holocene climatic change in
851 southwestern Spain: the Laguna de Medina, Cádiz, Holocene, 11, 707-719,
852 DOI:10.1191/09596830195735, 2001.
- 853 Reimer, P. J., Bard, E., Bayliss, A., Beck, J. W., Blackwell, P. G., Bronk Ramsey, C., Buck, C. E., Cheng,
854 H., Edwards, R. L., Friedrich, M., Grootes, P. M., Guilderson, T. P., Haflidason, H., Hajdas, I., Hatté, C.,
855 Heaton, T. J., Hoffmann, D. L., Hogg, A. G., Hughen, K. A., Kaiser, K. F., Kromer, B., Manning, S. W.,
856 Niu, M., Reimer, R. W., Richards, D. A., Scott, M., Southon, J. R., Staff, R. A., Turney, C. S. M., and van
857 der Plicht, J.: IntCal13 and Marine13 radiocarbon age calibration curves 0-50,000 years cal BP,
858 *Radiocarbon*, 55, 1869-1887, DOI:10.2458/azu_js_rc.55.16947, 2013.



- 859 Regattieri, E., Zanchetta, G., Drysdale, R. N., Isola, I., Hellstrom, J. C., Dallai, L.: Lateglacial to holocene
860 trace element record (Ba, Mg, Sr) from corchia cave (Apuan Alps, central Italy): paleoenvironmental
861 implications, *J. Quat. Sci.*, 29, 381-392, DOI:10.1002/jqs.2712, 2014.
- 862 Révillon, S., Jouet, G., Bayon, G., Rabineau, M., Dennielou, B., Hémond, C., and Berné, S.: The
863 provenance of sediments in the Gulf of Lions, western Mediterranean Sea, *Geochem. Geophys. Geosy.*,
864 12, Q08006, DOI:10.1029/2011GC003523, 2011.
- 865 Rodrigo-Gámiz, M., Martínez-Ruiz, F., Jiménez-Espejo, F. J., Gallego-Torres, D., Nieto-Moreno, V.,
866 Romero, O., Ariztegui, D.: Impact of climate variability in the western Mediterranean during the last
867 20,000 years: oceanic and atmospheric responses, *Quaternary Sci. Rev.*, 30, 2018-2034,
868 DOI:10.1016/j.quascirev.2011.05.011, 2011.
- 869 Sawatzky, C. L., Wurtsbaugh, W. A., Luecke, C.: The spatial and temporal dynamics of deep chlorophyll
870 layers in high-mountain lakes: effects of nutrients, grazing, and herbivore recycling as growth
871 determinants, *J. Plankton Res.*, 28, 65–86, DOI:10.1093/plankt/fbi101, 2006.
- 872 Schulte, L.: Climatic and human influence on river systems and glacier fluctuations in southeast Spain
873 since the Last Glacial Maximum, *Quatern. Int.*, 93-94, 85-100, DOI:10.1016/S1040-6182(02)00008-3,
874 2002.
- 875 Sánchez-López, G., Hernández, A., Pla-Rabes, S., Trigo, R. M., Toro, M., Granados, I., Sáez, A.,
876 Masqué, P., Pueyo, J. J., Rubio-Inglés, M. J., and Giral, S.: Climate reconstruction for the last two
877 millennia in central Iberia: The role of East Atlantic (EA), North Atlantic Oscillation (NAO) and their
878 interplay over the Iberian Peninsula, *Quaternary Sci. Rev.*, 149, 135-150,
879 DOI:10.1016/j.quascirev.2016.07.021, 2016.
- 880 Settle D. M., and Patterson C. C.: Lead in Albacore: guide to lead pollution in Americans, *Science*, 207,
881 1167-76, DOI:10.1126/science.6986654 ,1980.
- 882 Solanki, S. K., Usoskin, I. G., Kromer, B., Schüssler, M., and Beer, J.: Unusual activity of the Sun during
883 recent decades compared to the previous 11,000 years, *Nature*, 431, 1084-1087,
884 DOI:10.1038/nature02995, 2004.
- 885 Tjallingii, R., Röhl, U., Kölling, M., and Bickert, T.: Influence of the water content on X-ray fluorescence
886 core-scanning measurements in soft marine sediments, *Geoch. Geophys. Geosy.*, 8,
887 DOI:10.1029/2006GC001393, 2007.
- 888 Trigo, R. M., and Palutikof, J. P.: Precipitation scenarios over Iberia: a comparison between direct GCM
889 output and different downscaling techniques, *J. Climate* , 14, 4442-4446, DOI:10.1175/1520-
890 0442(2001)014<4422:PSOIAAC>2.0.CO;2, 2001.
- 891 Trigo, R. M., Pozo-Vázquez, D., Osborn, T. J., Castro-Díez, Y., Gámiz-Fortis, S., and Esteban-Parra, M.
892 J.: North Atlantic Oscillation influence on precipitation, river flow and water resources in the Iberian
893 Peninsula, *Int. J. Climatol.*, 24, 925-944, DOI:10.1002/joc.1048, 2004.



- 894 Trouet, V., Esper, J., Graham, N. E., Baker, A., Scourse, J.D., and Frank, D.C.: Persistent positive North
895 Atlantic Oscillation mode dominated the Medieval Climate Anomaly, *Science*, 324, 78-80,
896 DOI:10.1126/science.1166349, 2009.
- 897 Valbuena-Carabaña, M., López de Heredia, U., Fuentes-Utrilla, P., González-Doncel, I., and Gil, L.:
898 Historical and recent changes in the Spanish forests: a socioeconomic process, *Rev. Palaeobot. Palyno.*,
899 162, 492-506, DOI:10.1016/j.revpalbo.2009.11.003, 2010.
- 900 Valle, F.: *Mapa de series de vegetación de Andalucía 1: 400 000*, Editorial Rueda, Madrid, 2003.
- 901 Van der Weijden, C. H.: Pitfalls of normalization of marine geochemical data using a common divisor,
902 *Mar. Geol.*, 184, 167-187, DOI:10.1016/S0025-3227(01)00297-3, 2002.
- 903 Walczak, I. W., Baldini, J. U., Baldini, L. M., McDermott, F., Marsden, S., Standish, C. D., Richards, D.
904 A., Andreo, B., and Slater, J.: Reconstructing high-resolution climate using CT scanning of unsectioned
905 stalagmites: A case study identifying the mid-Holocene onset of the Mediterranean climate in southern
906 Iberia, *Quaternary Sci. Revi.*, 127, 117-128, DOI:10.1016/j.quascirev.2015.06.013, 2015.
- 907 Wanner, H., Brönnimann, S., Casty, C., Gyalistras, D., Luterbacher, J., Schmutz, C., Stephenson, D. B.,
908 and Xoplaki, E.: North Atlantic Oscillation—concepts and studies, *Surv. Geophys.*, 22, 321-381,
909 DOI:10.1023/A:1014217317898, 2001.
- 910 Wiersma, A. P., and Jongma, J. I.: A role for icebergs in the 8.2 ka climate event, *Climate dynamics*, 35,
911 535-549, DOI:10.1007/s00382-009-0645-1, 2010.
- 912 Wiersma, A. P., Roche, D. M., and Renssen, H.: Fingerprinting the 8.2 ka event climate response in a
913 coupled climate model, *J. Quat. Sci.*, 26, 118-127, DOI:10.1002/jqs.1439, 2011.
- 914 Yuan, F.: A multi-element sediment record of hydrological and environmental changes from Lake Erie
915 since 1800, *J. Paleolimnol.*, 58, 23-42, DOI:10.1007/s10933-017-9953-3, 2017.
- 916 Zanchetta, G., Drysdale, R. N., Hellstrom, J. C., Fallick, A. E., Isola, I., Gagan, M. K., Pareschi, M. T.:
917 Enhanced rainfall in the Western Mediterranean during deposition of sapropel S1: stalagmite evidence
918 from Corchia cave (Central Italy), *Quaternary Sci. Rev.*, 26, 279-286,
919 DOI:10.1016/j.quascirev.2006.12.003, 2007.
- 920
921
922
923
924
925
926
927
928
929
930



931 **List of tables**

<i>Lab Number</i>	<i>Depth (cm)</i>	<i>Dating Method</i>	<i>Age (14C yr BP±1σ)</i>	<i>Calibrated age (cal yr BP)2σ ranges</i>
	0	Present	2012 CE	-63
<i>Poz-72421</i>	7	14C	40±40	29-139
<i>D-AMS 008539</i>	22	14C	1112±32	935-1078
<i>D-AMS 008540</i>	39	14C	2675±30	2750-2809
<i>BETA-411994</i>	44	14C	3350±30	3550-3643
<i>BETA-411995</i>	55.5	14C	5480±30	6261-6318
<i>Poz-72423</i>	57.5	14C	5510±50	6266-6405
<i>Poz-72424</i>	62	14C	6450±50	7272-7433
<i>Poz-72425</i>	74	14C	8620±70	9479-9778

932 **Table 1.** Age data for LH 12-03. All ages were calibrated using IntCal13 curve (Reimer et al., 2013) with
 933 Clam program (Blaauw, 2010; version 2.2).

934

935

936

937

938

939

940

941

942

943

944

945

946

947

948

949

950

951



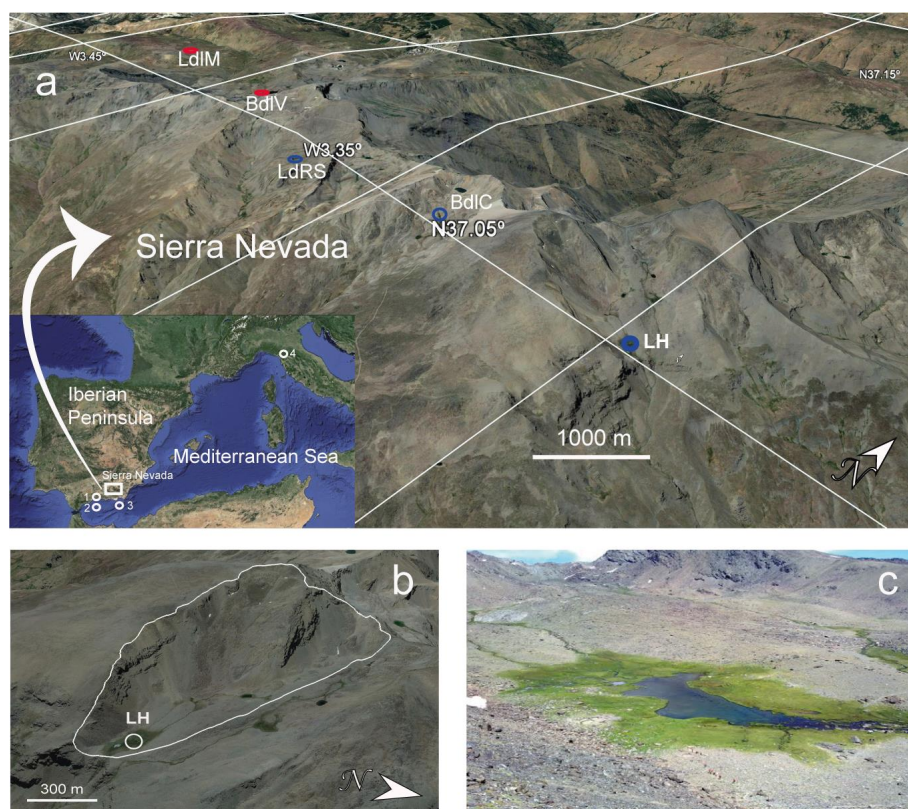
	Simulation							
Correlation	A		B		C		D	
Ca/Ca (XRF)	0.63	p<0.01	0.50	p<0.01	0.57	p<0.01	0.54	p<0.01
K/K (XRF)	0.53	p<0.01	0.64	p<0.01	0.56	p<0.01	0.65	p<0.01

952 **Table 2.** Simulation of proxy correlation. A) regular interpolation of 300 years sampling spacing. B)
 953 regular interpolation of 300 years sampling spacing and 5 data points moving average. C) regular
 954 interpolation of 150 years sampling spacing. D) regular interpolation of 150 years sampling spacing and 5
 955 data point moving average.

956
 957
 958
 959
 960
 961
 962
 963
 964
 965
 966
 967
 968
 969
 970
 971
 972
 973
 974
 975
 976
 977
 978
 979
 980
 981
 982
 983

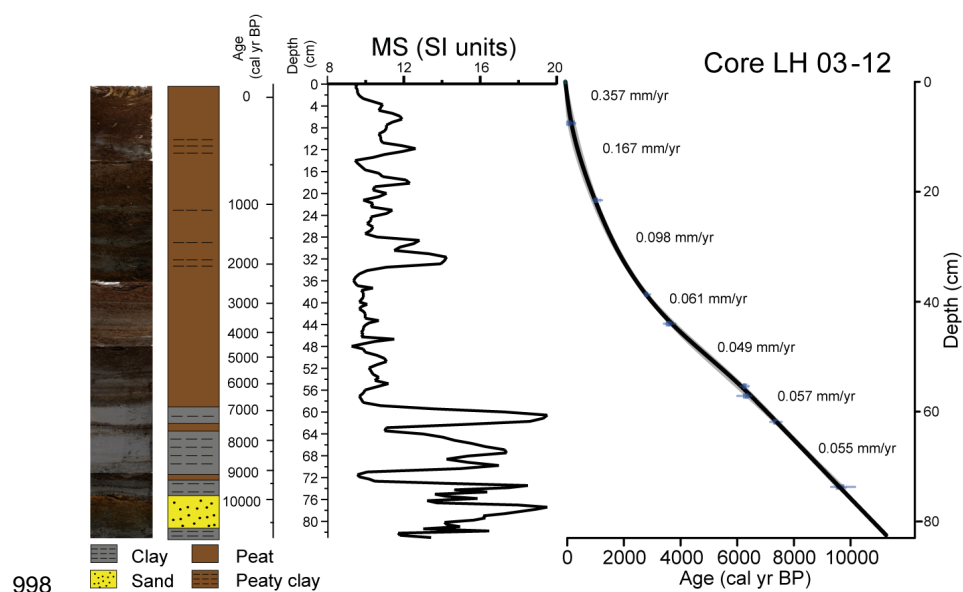


984 **List of figures**



985

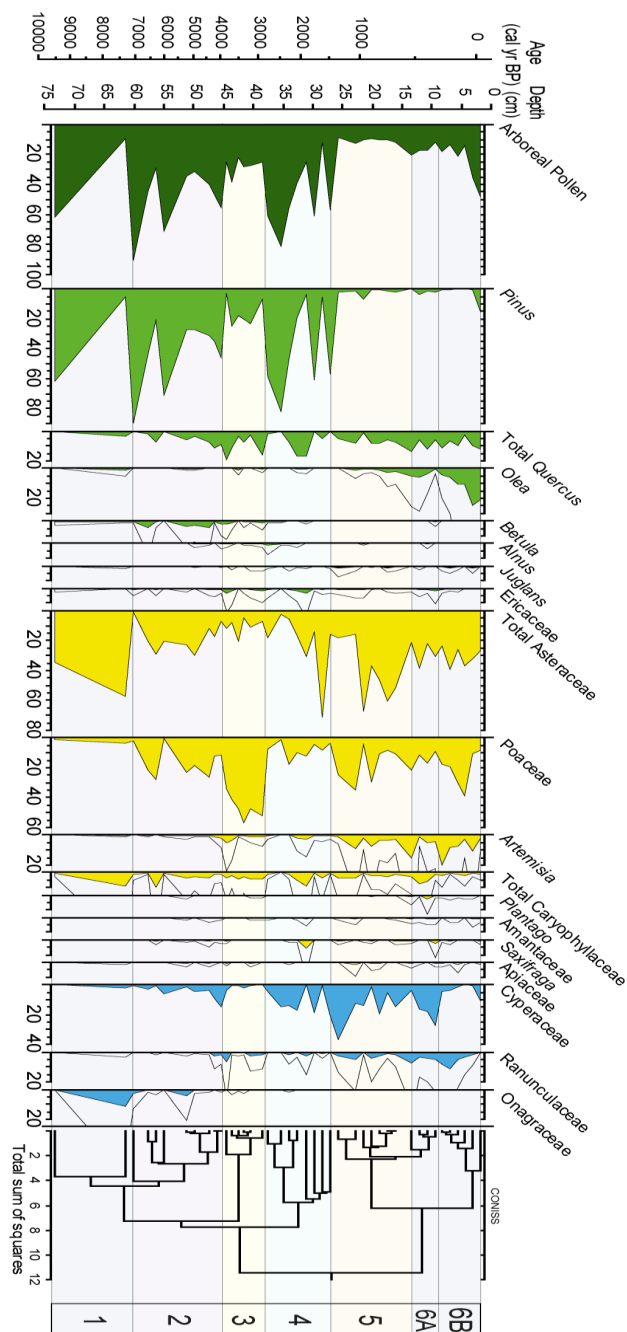
986 **Figure 1.** (a) Location of the Laguna Hondera (LH) in Sierra Nevada, southern Iberian Peninsula,
987 Mediterranean region, along with other nearby records mentioned in the text. (1) El Refugio Cave
988 stalagmite record; (2) ODP 976 pollen record (Combourieu-Nebout et al., 2009); (3) MD95-2043 pollen
989 record (Fletcher and Sánchez-Goñi, 2008); (4) CC26, Corchia Cave stalagmite record (Zanchetta et al.,
990 2007; Regattieri et al., 2014). Sierra Nevada north-facing sites are encircled in red, south-facing sites are
991 encircled in blue (LH: Laguna Hondera, the current study, is shown in bold). LdLM: Laguna de la Mula
992 (Jiménez-Moreno et al., 2013); BdLV: Borreguil de la Virgen (García-Alix et al., 2012; Jiménez-Moreno
993 and Anderson, 2012); LdRS: Laguna de Río Seco (Anderson et al., 2011; García-Alix et al., 2013;
994 Jiménez-Espejo et al., 2014); BdLC: Borreguil de la Caldera (Ramos-Román et al., 2016; García-Alix et
995 al., 2017) (b) Regional satellite photo of LH. The catchment area is indicated by the white line. (c) Photo
996 of Laguna Hondera in September 2012, when the core was taken. Photo taken by Gonzalo Jiménez-
997 Moreno



998

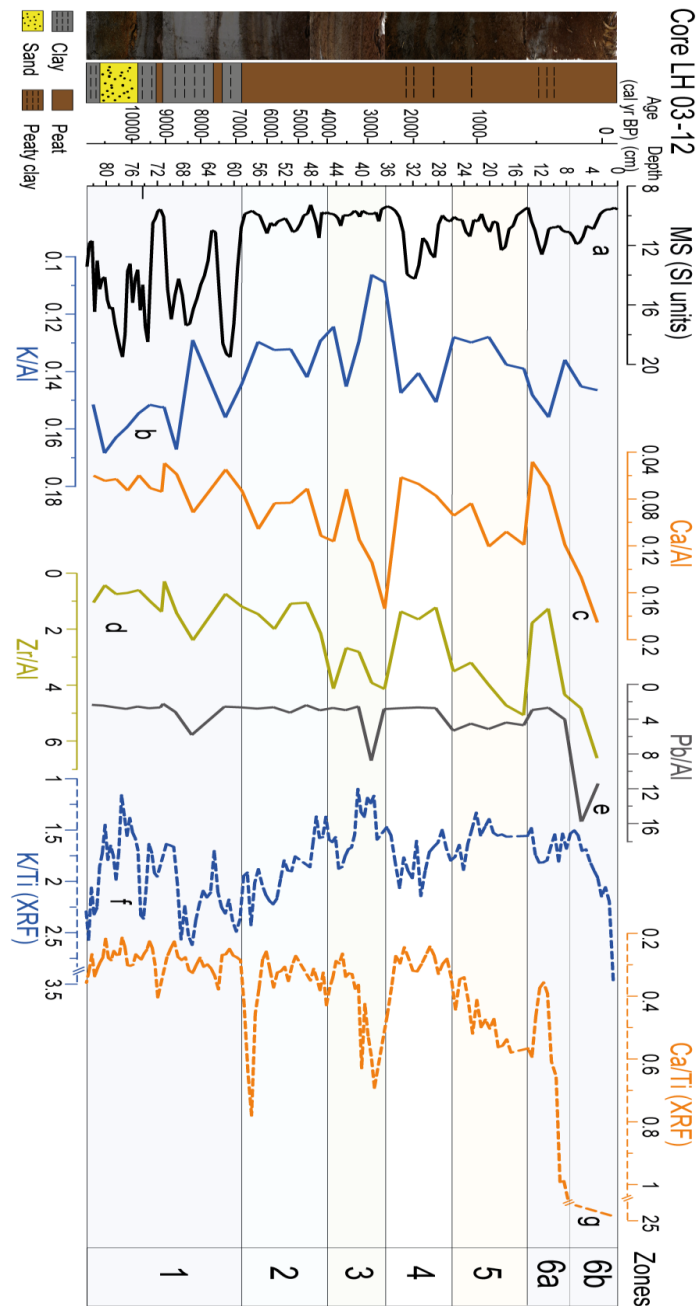
999 **Figure 2.** Photo of core LH 12-03, along with the lithology, magnetic susceptibility (MS, in SI units)
1000 profile and age-depth model. Sediment accumulation rates (SAR in mm yr^{-1}) are shown between
1001 individual radiocarbon ages (see details in text for method of construction).

1002



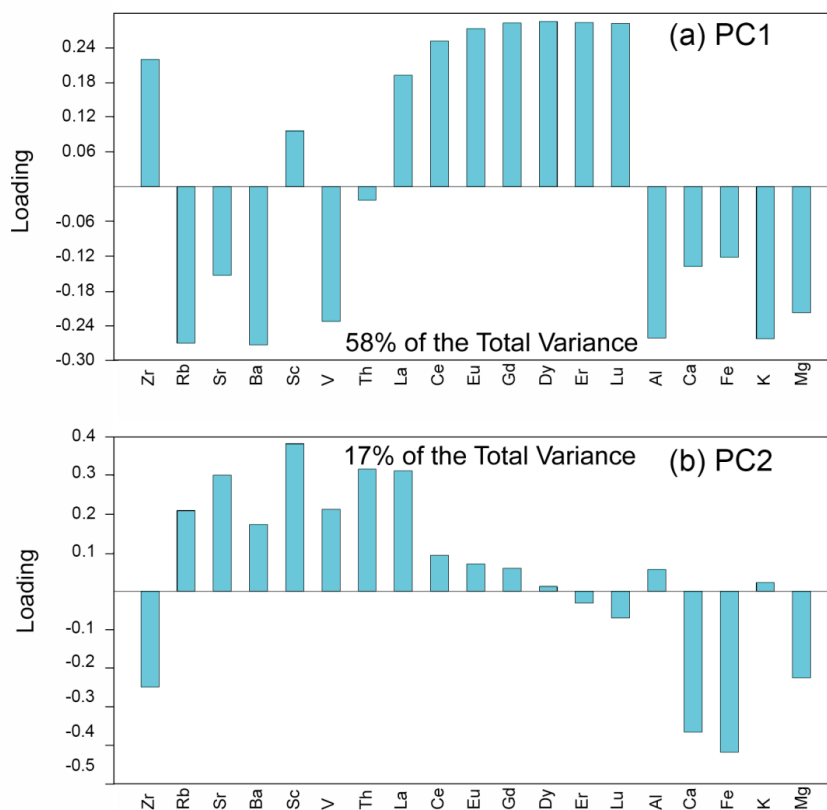
1003

1004 **Figure 3.** Pollen percentage diagram of the LH 12-03 record showing major selected taxa. Major tree
 1005 species are shown in green; shrubs and herbs are shown in yellow; and wetland and aquatic types are in
 1006 blue. Pollen was graphed with the Tilia program (Grimm, 1993), and zoned using the CONISS cluster
 1007 analysis program (Grimm, 1987).

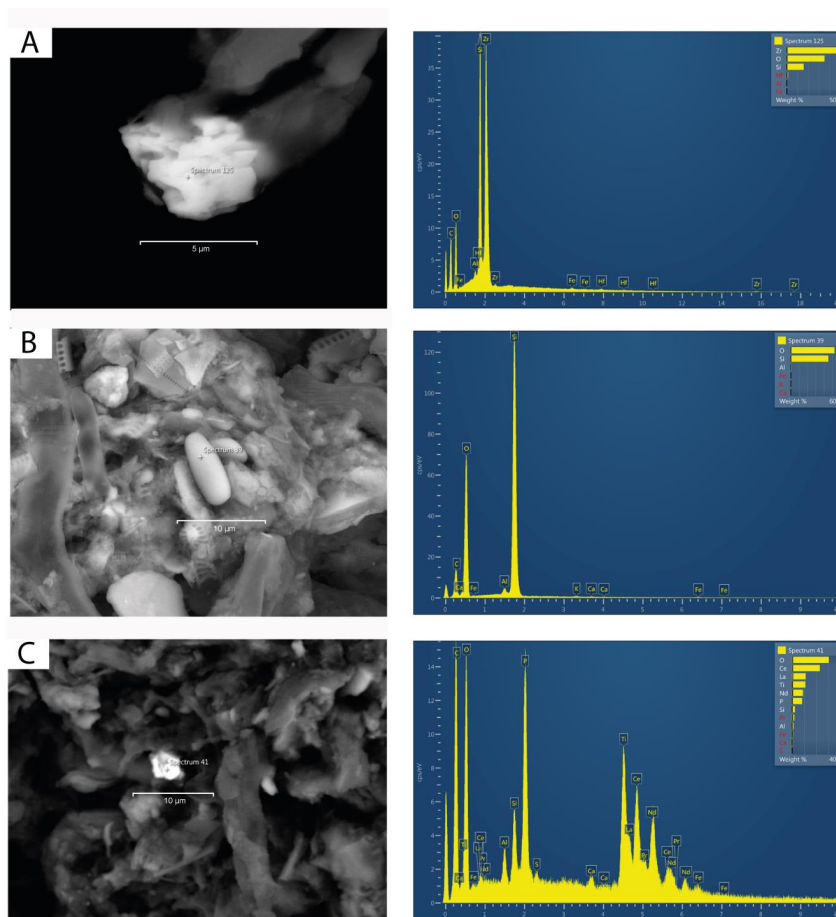


1008

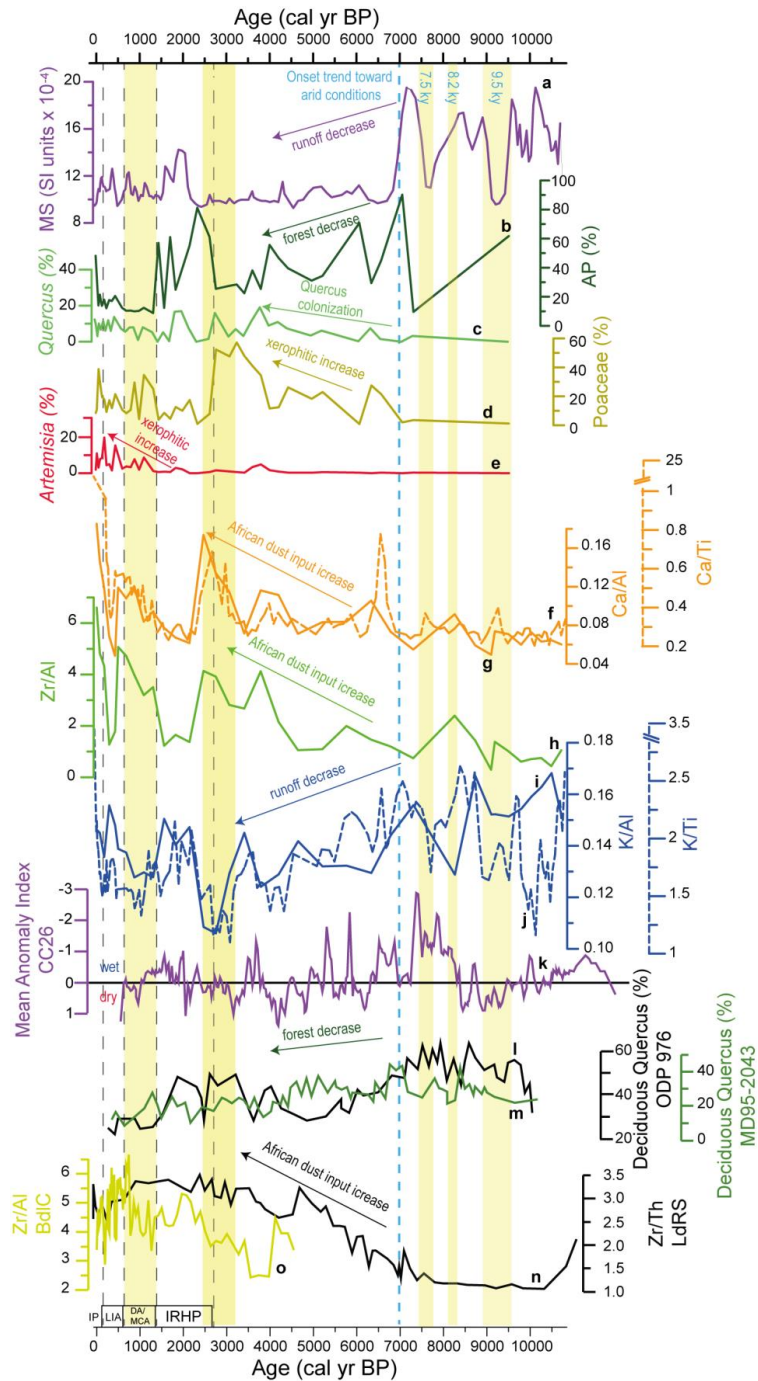
1009 **Figure 4.** Detailed geochemical diagram of the LH 12-03 record showing the selected proxies: (a) MS;
 1010 (b) K/Al; (c) Ca/Al; (d) Zr/Al; (e) Pb/Al; (f) K/Al (XRF); (g) Ca/Al (XRF) (MS in SI units, Zr/Al and
 1011 Pb/Al scale $\times 10^{-4}$ and XRF in counts). Pollen zonation described in section 4.3 was used.



1012
1013 **Figure 5.** Principal Component Analysis (PCA) loadings from selected geochemical elements. (a) PC1,
1014 which describes 58% of total variance; (b) PC2, which describes 17% of total variance.



1015
1016 **Figure 6.** Electron Backscatter Diffraction microphotographs of the LH record with clearer colours
1017 representing heavier minerals. (a) Zircon, with high Zr content (Dr. 01, 4-5 cm); (b) rounded quartz
1018 related with eolian transport (Dr. 01, 2-3 cm); (c) monazite, with high REE content (Dr. 01, 2-3 cm).



1019

1020 **Figure 7.** Comparison of MS data (in SI units $\times 10^{-4}$), the most important pollen taxa and geochemical
 1021 proxies from LH 12-03 record, with nearby paleoclimate records. (a) LH Magnetic Susceptibility (MS)
 1022 record; (b) Arboreal Pollen (AP) percentage from LH; (c) *Quercus* percentage from LH; (d) Poaceae



1023 percentage from LH; (e) Artemisia percentage from LH; (f) Ca/Ti (XRF) ratio from LH in dashed line;
1024 (g) Ca/Al ratio from LH; (h) Zr/Al ratio from LH; (i) K/Al ratio from LH; (j) K/Ti (XRF) ratio from LH
1025 in dashed line; (k) Mean Anomaly Index from CC26 record (Corchia cave; Regattieri et al., 2014); (l)
1026 Deciduous *Quercus* ODP 976 (Alboran Sea; Combourieu-Nebout et al., 2009); (m) Deciduous *Quercus*
1027 MD95-2043 (Alboran Sea; Fletcher and Sanchez-Goñi, 2008); (n) Zr/Th ratio from Laguna de Río Seco
1028 (LdRS); (o) Zr/Al ratio from Borreguil de la Caldera (BdlC). Yellow bands indicate more arid intervals.
1029 Dark dashed lines are used for separating the different CE periods: IRHP: Iberian Roman Humid Period;
1030 DA: Dark Ages; MCA: Medieval Climate Anomaly; LIA: Little Ice Age; IP: Industrial Period. Blue
1031 dashed line indicates the onset of the trend toward arid conditions.

1032

1033

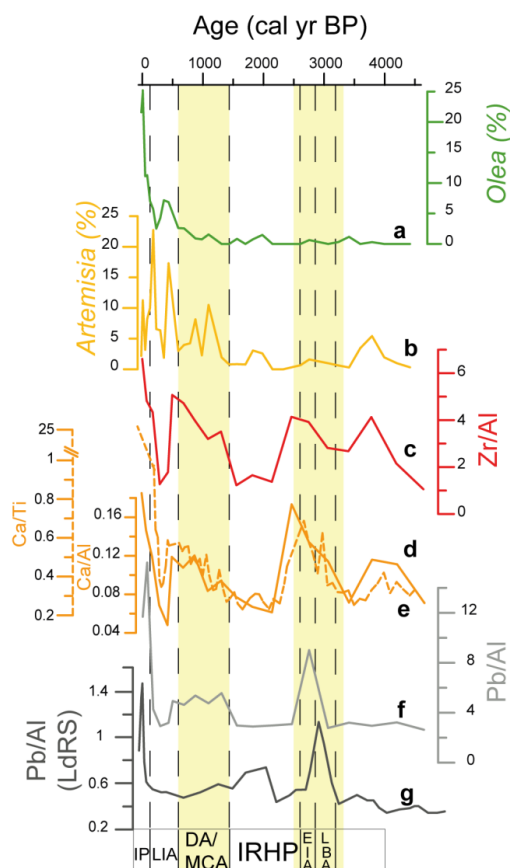
1034

1035

1036

1037

1038



1039

1040 **Figure 8.** Comparison of geochemical proxies with pollen taxa, related to anthropogenic impact for the
 1041 last ~4500 cal yr BP. (a) *Olea* percentage from LH; (b) *Artemisia* percentage from LH record; (c) Zr/Al
 1042 ratio from LH; (d) Ca/Al ratio from LH; (e) Ca/Ti (XRF) ratio from LH; (f) Pb/Al ratio from LH; (g)
 1043 Pb/Al ratio from Laguna de Río Seco (LdRS). Yellow bands indicate more arid intervals. Dark dashed
 1044 lines are used for separating the different CE and BCE periods: LBA: Late Broze Age; EIA: Early Iron
 1045 Age; IRHP: Iberian Roman Humid Period; DA: Dark Ages; MCA: Medieval Climate Anomaly; LIA:
 1046 Little Ice Age; IP: Industrial Period.